Ice and Supercooled Liquid Water Distributions over the Southern Ocean based on In Situ Observations and Climate Model Simulations

Ching An Yang[1], Minghui Diao[1,*], Andrew Gettelman[2], Kai Zhang[3], Jian Sun[3]

[1]Department of Meteorology and Climate Science, San Jose State University, One Washington Square, San Jose, California, USA, 95192-0104

[2]National Center for Atmospheric Research, 3450 Mitchell Ln, Boulder, CO, USA, 80301

[3]Pacific Northwest National Laboratory, 902 Battelle Blvd, Richland, WA, USA, 99354

*Corresponding author:

Minghui Diao, Ph.D., Associate Professor

Email: Minghui.diao@sjsu.edu

Key Points

- Model biases of cloud occurrences and cloud phases are correlated with RH biases.
- Positive correlations are observed between aerosol concentrations and LWC, IWC, N_{liq}, N_{ice}, glaciation ratio, and cloud fraction.
- CAM6 and E3SM show higher (lower) LWC (IWC) by a factor of 3–100 (3–10) and weaker aerosol indirect effects than 100-km scale observations.

Abstract

An evaluation of three climate models is conducted using in situ airborne observations from the Southern Ocean Clouds, Radiation, Aerosol Transport Experimental Study (SOCRATES) campaign. The evaluation targets cloud phases, microphysical properties, thermodynamic conditions, and aerosol indirect effects at -40°C – 0°C. For cloud phase frequency distribution, the Community Atmosphere Model version 6 (CAM6) shows the most similar result to the observations, which allows more liquid-containing clouds below -10°C compared with its predecessor – CAM5. The Energy Exascale Earth System Model (E3SM) underestimates (overestimates) ice phase frequencies below (above) -20°C. Compared with 580-second averaged observations (i.e., 100 km horizontal scale), CAM6 and E3SM overestimate (underestimate) liquid (ice) water content (i.e., LWC and IWC), leading to lower a glaciation ratio when ice and liquid coexist. Thermodynamic conditions, specifically relative humidity (RH), is likely a key factor contributing to model cloud occurrence and cloud phase biases. Simulated in-cloud RH shows higher minimum values than observations, possibly restricting ice growth during sedimentation. As number concentrations of larger and smaller aerosols (> 500 nm and > 100 nm) increase, observations show increases in glaciation ratio, cloud fraction, LWC and liquid number concentration (N_{liq}) at -18ºC to 0ºC, and IWC and ice number concentration (N_{ice}) at -35ºC to 0ºC. CAM6 and E3SM show slight increases of LWC and N_{liq}, and E3SM shows small increases of N_{ice}. These results indicate that models underestimate aerosol indirect effects on ice and mixed phase clouds over the Southern Ocean.

Plain Language Summary

Clouds can be collections of entirely liquid droplets, ice particles, or both. Thermodynamic phase of clouds, particularly in the Southern Ocean, contributes to large uncertainties in climate model simulations. This study uses aircraft observation data to evaluate the performance of three climate models. The evaluation compares model simulations with the observation data in terms of environmental conditions (temperature and relative humidity), microphysical properties (amount of liquid and ice), and the relationship between aerosols and clouds at temperatures from -40°C to 0°C. CAM5 does not allow supercooled liquid water below -10°C, while a newer version – CAM6, improves the result by showing distributions of three cloud phases comparable to observations. E3SM, on the other hand, has too many (few) number of liquid (ice) clouds at -35°C to -20°C. All three models show an insufficient amount of ice than the observations. Model biases of cloud occurrences and cloud phase are found to correlate with biases in relative humidity. The observations show strong relationships between aerosols and cloud properties. As aerosol number concentration increases, observations show higher cloud fraction, more ice crystals and supercooled liquid droplets. The models show weaker aerosol indirect effects compared with observations.

Keywords:

Ice and mixed phase clouds; Southern Ocean; In situ observations; Cloud phase; CAM model; E3SM model.

1. Introduction

Clouds reflect shortwave radiation and re-emit terrestrial longwave radiation. They play a crucial role in influencing Earth's radiation budget (Liou, 1992). The cloud types, height, the partition of cloud phases, and microphysical properties of liquid droplets and ice crystals are found to be important in determining the cloud radiative effect (Chen et al., 2000; Matus & L'Ecuyer, 2017).

Mixed phase clouds, clouds with the coexistence of liquid and ice, have been a focus of cloud microphysics research as many of their properties remain not fully understood (e.g., Korolev et al., 2017; Lohmann et al., 2016). A frequently occurring process in mixed phase clouds, named the Wegener-Bergeron-Findeisen (WBF) process, describes ice crystal growth at the expense of liquid droplets as the liquid droplets evaporate to water vapor that deposits on ice crystals (Wegener, 1912; Bergeron, 1928). This occurs when ambient water vapor partial pressure (e) is lower than the saturation vapor pressure with respect to liquid ($e_{s,liq}$) but higher than the saturation vapor pressure with respect to ice ($e_{s,ice}$). The amount of ice and liquid and their mass partition in mixed phase clouds are crucial for determining cloud lifetime, radiative properties, and precipitation (Mülmenstädt et al., 2015; Morrison et al., 2010), as well as for developing model parameterizations that represent these properties (e.g., Tan & Storelvmo, 2016; M. Zhang et al., 2019).

Supercooled liquid water, i.e., liquid droplets that exist below 0°C in both liquid and mixed phase clouds, was previously found to be underestimated in several global climate model (GCM) simulations, particularly in the Southern Ocean (Bodas-Salcedo et al., 2016; Williams et al., 2013; Tan et al., 2016; McCoy et al., 2016). Due to the scarcity of in situ observations in remote regions

such as the Southern Ocean, many evaluations of model biases rely on satellite observations (e.g., Trenberth & Fasullo, 2010; Kay et al., 2012). Guo et al. (2020), as an example, used satellite retrieval data from Cloud-Aerosol Lidar and Infrared Pathfinder Satellite Observation (CALIPSO) to compare with the Community Atmosphere Model version 5 (CAM5). They concluded that the model misclassifies liquid as ice, leading to an underestimation of liquid cloud occurrence frequencies and an overestimation of ice cloud occurrence frequencies in all vertical levels. The model also shows that the supercooled liquid fraction reaches 50% at -5°C, which is much warmer than the observed value of -20°C. When comparing with airborne observations around Punta Arenas, Chile, D'Alessandro et al. (2019) showed that the CAM5 does not allow liquid and mixed phase clouds to exist below -15°C. The model was found to overestimate and underestimate liquid water content (LWC) in liquid and mixed phases, respectively, and underestimate ice water content (IWC) in ice and mixed phases, which demonstrates the importance of separating three cloud phases for model evaluation. Another study compared ground-based observations of mixed phase clouds over the Arctic with the CAM5, and showed that revising the mixing volumes where supercooled liquid water and ice particles coexist in the model can reduce the effectiveness of WBF process, which prolongs the lifetime of supercooled liquid water (M. Zhang et al., 2019). Klein et al. (2009) found an underestimation of the median liquid water path by a factor of three in single-column models and cloud-resolving models when comparing with the observations from Mixed-Phase Arctic Cloud Experiment (M-PACE). That study emphasized the importance of ice microphysical processes, such as ice initiation and water vapor deposition rate on ice crystals, which contribute to the underestimation of the liquid water path.

Thermodynamic (i.e., temperature and relative humidity), dynamic (i.e., wind speed and direction), and aerosol concentration and composition are crucial for the existence of supercooled

liquid water (D'Alessandro et al., 2019; Fan et al., 2011; Korolev & Isaac, 2006; Gierens et al., 2020; D. Zhang et al., 2019). Previously, studies showed ice, liquid and mixed phase clouds have distinct relative humidity distributions. That is, relative humidity with respect to liquid (RH_{liq}) in liquid clouds is close to liquid saturation, while relative humidity with respect to ice (RH_{ice}) in ice clouds can deviate more from ice saturation (Fan et al., 2011; Korolev & Isaac, 2006; D'Alessandro et al., 2019). For mixed phase clouds, D'Alessandro et al. (2019) showed increasing deviations of RH_{liq} from liquid saturation as ice mass fraction increases in the mixture of ice and liquid. Other studies also found that mixed phase clouds are influenced by vertical velocity (e.g., Korolev & Field, 2008; Shupe et al., 2008; Bühl et al., 2019) and horizontal wind direction (e.g., Gierens et al., 2020; Qiu et al., 2018) from the microscale to mesoscale. For example, Shupe et al. (2008) showed that an in-cloud updraft of 0.4 m s^{-1} can sustain mixed-phase stratiform clouds in the Arctic, and both cloud liquid and ice mass grow inside updrafts. Korolev and Field (2008) showed that the generation of mixed-phase clouds in an ice cloud parcel requires two necessary conditions for vertical velocity in theory – activating liquid water as well as increasing e to $e_{s,liq}$. Bühl et al. (2019) showed that higher fluctuations in vertical velocity can lead to increasing ice mass flux via primary ice production. Gierens et al. (2020) and Qiu et al. (2018) found that mixed phase clouds occur more frequently in certain wind direction at Ny Ålesund, Arctic and Utqiaġvik, Alaska.

Aerosol number concentration and size distribution are also known to influence the formation and evolution of ice particles and supercooled liquid water. Three hypothesized aerosol indirect effects for mixed phase clouds are: (i) the glaciation indirect effect, which describes increases of ice nucleating particles (INPs) that lead to more ice particles and ice phase precipitation (Lohmann, 2002); (ii) the riming indirect effect, which describes increases of cloud

condensation nuclei (CCN) concentrations that lead to smaller liquid droplets, less riming and smaller IWC (Borys et al., 2003); and (iii) the thermodynamic indirect effect, which describes increases of CCN concentrations that lead to more liquid droplets, less secondary ice production (Hallett & Mossop, 1974) and fewer ice particles (Rangno & Hobbs, 2001). Using airborne observation data, Jackson et al. (2012) found a positive correlation between liquid number concentration inside clouds and aerosol number concentration below clouds. They also found a positive correlation between ice number concentration and aerosol number concentration above clouds. Storelvmo et al. (2011) conducted a modeling study for aerosol indirect effects on mixed phase clouds and found decreasing cloud lifetime due to increasing INP concentrations. They also found decreasing ice particle sizes and increasing cloud albedo due to increasing INP concentrations, which is similar to the Twomey effect on liquid clouds. These studies demonstrated the importance of thermodynamic conditions and aerosol indirect effects on cloud microphysical properties in the mixed phase cloud regime.

This study examines ice particle and supercooled liquid water distributions over the Southern Ocean based on the Southern Ocean Clouds, Radiation, Aerosol Transport Experimental Study (SOCRATES), and compares in situ observations with simulations of three GCMs: the National Center for Atmospheric Research (NCAR) Community Atmosphere Model version 5 (CAM5) and version 6 (CAM6), and the Energy Exascale Earth System Model (E3SM) by the U.S. Department of Energy (DOE). CAM5 and CAM6 are the atmospheric component of the NCAR Community Earth System Model version 1 (CESM1) and version 2 (CESM2), respectively. Compared with CAM5, CAM6 has improvements applied to mixed phase cloud parameterization, prognostic precipitation species, and the interaction with aerosol schemes. E3SM uses a similar physics package as CAM6 but includes many differences, such as a different dynamical core, more

vertical levels, a more detailed treatment of aerosol variety and properties, etc. The main goals of this work are to advance the understanding of statistical distributions of cloud phase and microphysical properties, the thermodynamic effect, and aerosol indirect effects on cloud characteristics over the Southern Ocean, as well as to provide evaluations on three model simulations.

In Section 2, the observation dataset and the set-up of model simulations are introduced. In Section 3, case studies of three cloud segments are presented, and their thermodynamic conditions (e.g., temperature and RH), cloud phases, and cloud microphysical properties are compared between the observations and model simulations. Statistical distributions of cloud phase occurrence frequencies, mass and number concentrations of cloud hydrometeors, effects of thermodynamic conditions, and aerosol indirect effects are also analyzed based on a synthesized observation dataset. Lastly, conclusions and implications are given in Section 4.

2. Instrumentations and Simulations

2.1 In situ airborne observations

The SOCRATES campaign is a flight campaign funded by the U.S. National Science Foundation (NSF) and supported by NCAR. The campaign was conducted over the Australasian section of the Southern Ocean region located at 62°S – 42°S and 133°E – 164°E, from January 15 to February 24, 2018. The SOCRATES campaign aims to study clouds, aerosols, cloud-aerosol interaction, precipitation, and radiation over the remote region of the Southern Ocean, where climate models tend to underestimate the shortwave radiation reflected by the low-level clouds in the Austral summer, especially in the colder sector of low-pressure systems. The research flights often targeted cyclonic and frontal systems where the presence of strong westerly and

172 southwesterly flows along with the cold ocean surface temperatures favor the formation of low-
173 level and mid-level clouds such as stratocumulus. For this analysis, temperatures are restricted to
174 -40°C – 0°C (also referred to as the mixed phase cloud regime hereafter), which allows for the
175 presence of both supercooled liquid water and ice particles. The SOCRATES campaign provides
176 a total of 15 research flights and 111 total flight hours at all temperatures. Among these
177 observations, 14 and 73 flight hours were at in-cloud and clear-sky conditions at -40°C – 0°C, with
178 average true airspeed at 156 and 178 m s^{-1}, respectively.

179 The NSF Gulfstream-V (GV) research aircraft is the platform used in the SOCRATES
180 campaign, with scientific instruments equipped to collect a series of data, including meteorological
181 conditions, cloud hydrometeors, total aerosol number concentrations, etc. A Rosemount
182 temperature probe measures temperature data, with an accuracy and precision of ±0.3 K and 0.01
183 K, respectively. The Fast-Two Dimensional Cloud probe (Fast-2DC) and cloud droplet probe
184 (CDP) were mounted underneath the aircraft wings to measure cloud properties including LWC,
185 IWC, and liquid and ice number concentrations (N_{liq} and N_{ice}) at 1-Hz resolution. The CDP
186 measures particle sizes from 2 to 50 μm, while Fast-2DC measures larger particle sizes from 62.5
187 to 1600 μm. In addition, the Fast-2DC probe mathematically reconstructs particles up to 3200 μm.
188 The Fast-2DC probe also captures particle images with a resolution of 25 μm by recording the
189 shadows of hydrometeors as they pass through a laser beam. Mounted next to the Fast-2DC, the
190 Ultra-High Sensitivity Aerosol Spectrometer (UHSAS) measures the number concentrations and
191 size distributions of aerosols in the 60 to 1000 nanometer (nm) range. Another instrument, the
192 Vertical Cavity Surface Emitting Laser (VCSEL) hygrometer, was mounted on top of the aircraft
193 and reported water vapor molecule number density at 25-Hz resolution with an accuracy of ~6%
194 and a precision of ≤ 1% (Zondlo et al., 2010). Its product of water vapor mixing ratio was reported

in 1-Hz resolution, and a PI-calibrated dataset of water vapor mixing ratio is used in this study based on post-campaign laboratory calibration in summer 2018 (Diao, 2020). Water vapor and temperature data are used to calculate RH_{liq} and RH_{ice} by using the equations for $e_{s,liq}$ and $e_{s,ice}$ in Murphy and Koop (2005), respectively. Combining the uncertainties from water vapor and temperature measurements, the uncertainties for RH_{ice} are 6.9% – 6.5%, and the uncertainties for RH_{liq} are 6.8% – 6.4% from -40°C to 0°C, respectively.

The observed cloud phases are determined based on the cloud phase identification method from Figure 1 of D'Alessandro et al. (2019). Measurements from CDP are categorized into three types (i.e., large aerosols, liquid droplets, and ice particles) based on various thresholds of particle number concentration (Nc_{CDP}) and mass concentration (Mc_{CDP}). That is, particles with $Nc_{CDP} \leq 10^{-1.5}$ cm^{-3} and $Mc_{CDP} \leq 10^{-3.4}$ g m^{-3} are considered large aerosols; particles with $10^{-1.5} < Nc_{CDP} < 10^{-0.5}$ cm^{-3} and $Mc_{CDP} > 10^{-3.4}$ g m^{-3} are defined as ice particles; and particles with $Nc_{CDP} \geq 10^{-0.5}$ cm^{-3} and $Mc_{CDP} > 10^{-3.4}$ g m^{-3} are defined as liquid droplets. For the Fast-2DC probe, if the ambient temperature ≥ -30°C, particle number concentration (Nc_{2DC}), the maximum particle diameter (D_{max_2DC}), and the standard deviation of size distribution (σ_{D_2DC}) are used to categorize liquid droplets and ice particles. If the ambient temperature < -30°C, a check of CDP reading is also required. The total LWC and IWC are based on the combined measurements of both probes. Cloud phases are defined by using the mass fraction of ice (hereafter named as the glaciation ratio), i.e., IWC/CWC, where CWC stands for cloud water content and equals the sum of LWC and IWC (Korolev and Isaac, 2003; D'Alessandro et al. 2019). Ice, mixed and liquid phases are defined when glaciation ratio > 0.9, 0.1 ≤ glaciation ratio ≤ 0.9, and glaciation ratio < 0.1, respectively.

2.2 Three GCM simulations

This study evaluates three model simulations against the in situ observations, including the NCAR CESM1 / CAM5 model, an updated version CESM2 / CAM6 model, and the DOE E3SM / Atmosphere Model version 1 (EAMv1). Figure 1 shows the map of aircraft flight tracks and the collocated model output from three simulations.

Both CAM5 and CAM6 use a finite-volume dynamical core (Lin et al., 2004). The two models were run with a resolution of 0.9° × 1.25° and 32 vertical levels, a time step of 30 minutes, and were nudged towards MERRA-2 temperature and horizontal wind field reanalysis data. The model output was saved at the closest location to the aircraft flight track for every 10-minute observations, which facilitates a more direct comparison between the simulations and observations. Both CAM5 and CAM6 were run with a spin-up time of one year, and a relaxation time of 24 hours when nudged towards the reanalysis data. The CAM5 simulation uses the MG1 cloud microphysics scheme (Morrison & Gettelman, 2008) coupled with a modal aerosol module with three modes (MAM3) (Liu et al., 2012). A detailed description of CAM5 was previously documented in Neale et al. (2012). The newer version, CAM6, uses cloud microphysics scheme MG2 with additional improvements of ice nucleation, ice microphysics, prognostic precipitation species, and interaction with aerosol schemes to calculate cloud mass fractions and number concentrations (Gettelman & Morrison, 2015). The MG2 microphysics scheme is coupled with an updated modal aerosol module with four modes, MAM4 (Liu et al., 2016). The MAM4 has an additional aerosol mode named primary carbon compared with MAM3, and has improvements to aerosol resuspension, nucleation, scavenging, and sea spray emissions. CAM6 also uses Cloud Layers Unified By Binormals (CLUBB) for turbulence and shallow convection, which replaces the original shallow convection scheme in CAM5 (Park & Bretherton, 2009).

The DOE E3SM / EAM version 1, on the other hand, is a derivative of CAM6 with a spectral element dynamical core and modified physics parameterization schemes (Rasch et al., 2019). The vertical and horizontal resolutions of E3SM are 72 layers and ne30 (1°), respectively. A nudged simulation towards ERA5 temperature and horizontal wind was performed, with a relaxation time scale of 6 hours (Sun et al., 2019). The output closest to flight track location at a 10-minute frequency is used for the comparison. The E3SM nudged simulation started on December 1, 2017 and was initialized with the initial condition output for December from a climatological run (for both atmosphere and land). This allows a relatively short simulation time for the model to spin up compared with using the default initial condition file. Similar to CAM6, E3SM also uses the MG2 microphysics scheme and MAM4, but with more detailed treatments of aerosol categories and processes such as light-absorbing particle deposition.

2.3 Approaches to facilitate comparisons between model simulations and observations

Due to differences of spatiotemporal resolutions and various definitions of cloud and aerosol variables between in situ observations and model simulations, several approaches are used to select collocated samples and recalculate model output variables for comparisons. First, for model output in an entire atmospheric column, only the model grid box with the closest location to the vertical location of the aircraft is selected. Second, since simulated cloud hydrometeors in the model cover the size range from zero to infinity, which exceeds the sampling range of CDP and Fast-2DC probes, a size cutoff is applied to all simulated cloud properties by restricting the particle size to a discrete range of 2 to 50 μm plus 62.5 to 3200 μm. This method was previously used in several model-observation comparison studies, such Eidhammer et al. (2014) and Patnaude et al. (2020). The model output variables being processed for this partial size range include “LWC”, “NUMLIQ”, “IWC”, “NUMICE”, “AQSNOW” and “ANSNOW”. These variables represent grid-

262 average values for mass and number concentrations of liquid, ice, and snow, respectively. The
263 simulated LWC and N_{liq} are defined by the size-restricted "LWC" and "NUMLIQ", respectively.
264 We further define the simulated IWC as the sum of size-restricted "IWC" and "AQSNOW" and
265 the simulated N_{ice} as the sum of size-restricted "NUMICE" and "ANSNOW", which means that
266 the simulated ice phase includes both ice crystals and snow since cloud measurements in the
267 observations include both ice crystals and snow. Aerosol number concentrations (Na) from the
268 simulations are also restricted to aerosol sizes ≤ 1000 nm based on a log-normal distribution, which
269 follows the size range of the UHSAS measurements. The RH_{ice} and RH_{liq} values in the simulations
270 are calculated based on water vapor specific humidity and the saturation vapor pressure equations
271 from Murphy and Koop (2005), which avoids using the RH variable directly reported by the model.
272 The simulated RH_{liq} shows the maximum values at 101%, 100%, and 105% for CAM6, CAM5,
273 and E3SM, respectively. For the observations, RH_{liq} values greater than 105% are set as NAN
274 values (processed for 2535 seconds) due to the combined uncertainties from water vapor and
275 temperature measurements. For in-cloud conditions, the observations define them as where at least
276 one cloud hydrometeor has been detected by either CDP or Fast-2DC probe. The maximum and
277 minimum values of LWC (IWC) in the observations are 1.41 and 5.01×10^{-5} g m^{-3} (55.79 and
278 5.68×10^{-5} g m^{-3}), respectively. For simulations, if IWC or LWC is less than 10^{-7} g m^{-3}, they are not
279 considered as real hydrometeors and are set to zero. This means that for simulations, in-cloud
280 conditions are defined as either IWC or LWC being greater than 10^{-7} g m^{-3}, while the remaining
281 conditions are considered as clear sky. In addition, only N_{liq} and N_{ice} greater than 10^{-7} cm^{-3} are
282 used in the analysis of simulations. Table 1 summarizes the maximum and minimum values for
283 thermodynamic conditions (i.e., temperature, pressure, RH_{ice}, and RH_{liq}) and cloud microphysical
284 properties (i.e., LWC, IWC, N_{liq}, and N_{ice}) used for the analysis of observations and simulations.

To examine the effect of spatial scales to the comparison results, 1-Hz observations are averaged by various scales, including 200 seconds (i.e., 34.5 km horizontal resolution, since the average true airspeed of the aircraft at -40°C to 0°C is 172 m s^{-1}) and 580 seconds (i.e., 100 km horizontal resolution) using a moving average method similar to D'Alessandro et al. (2019). This moving average generally leads to smaller values of average IWC, LWC, N_{ice}, and N_{liq} in coarser scale data compared with the 1-s data, since the coarser scale data include both clear-sky and in-cloud segments during the averaging process. Since these observation data represent averages over the entire length scale, they are comparable with simulated grid-average cloud quantities.

3. Results

3.1 Three case studies of cloud phases, microphysical properties and thermodynamic conditions

Individual flight segments from the SOCRATES campaign are selected to illustrate three typical situations: (i) an ice-dominated condition, (ii) a liquid-dominated condition, and (iii) a heterogeneous mixture of ice, liquid, and mixed phases.

A segment from research flight (RF) 04 represents a homogeneous segment of ice phase (Figures 2 and 3). The thermodynamic condition for this segment is ideal for ice formation with a temperature constantly around -32°C and the magnitude of ice supersaturation (i.e., $RH_{ice} - 1$) around 10% – 50% (Figure 2 a). The IWC values, derived from the 1-Hz CDP and 2DC measurements, are above 0.01 g m^{-3} for most of the in-cloud conditions (Figure 2 b). The 2DC imageries of cloud hydrometeors confirm ice phase samples defined by the cloud phase identification method (Figure 2 d and e).

The model simulations either miss part of the in-cloud segment or misidentify the cloud phase (Figure 2 c). These biases are well correlated with biases seen in the RH conditions (Figure 3 b and c). The CAM6 misses the first 7 minutes (UTC 00:43:00 – 00:50:00) of the in-cloud segment but overestimates IWC in a later segment (UTC 01:03:20 – 01:06:40) when it should be clear sky. CAM5 captures the ice phase in the beginning, possibly attributed to the simulated RH_{ice} by CAM5 being closer to observations than CAM6 at this time range. Even though E3SM shows smaller temperature biases than CAM6 and CAM5, it misses the in-cloud segment in the first 16 minutes (UTC 00:43:00 – 00:59:00) and also misidentifies the observed ice phase as mixed phase. These two biases shown in E3SM are correlated with a low RH_{ice} bias of 60% in the earlier segment and a high RH_{ice} bias of 20% – 50% at the later segment, respectively. In fact, in the later segment, E3SM shows RH_{liq} at liquid saturation, which produces false LWC at 0.03 g m^{-3} and N_{liq} at 5 cm^{-3} that should have been zero (Figure 3 e and g). Compared with 1-s observations, simulated IWC is 2 orders of magnitude smaller in CAM5, and 3 orders of magnitude smaller in CAM6 and E3SM between 00:50:30 and 01:01:00. Simulated N_{ice} in CAM5 is one order of magnitude higher than observations for the middle part of the segment, while CAM6 and E3SM show similar N_{ice} to the 1-s observations. Glaciation ratios of CAM5 and CAM6 follow the observed value at unity for ice phase, while E3SM shows very low glaciation ratios due to the false values of LWC at the later segment.

A segment from RF06 was selected to show a liquid-dominated segment with relatively homogeneous distributions of supercooled liquid water in UTC 02:31:40 – 02:43:00 (Figures 4 and 5). In this case, the observed temperature ranges from -2°C to -4°C and the RH_{liq} remains at or slightly below liquid saturation (Figure 4 a), favoring the existence of supercooled liquid water. All models have temperature and RH well matched with the observations (Figure 5 a – c), yet

differences in simulated IWC and LWC (Figure 5 d and e) lead to varying results of cloud phases. That is, E3SM simulates mixed phase for the entire segment while CAM5 and CAM6 show both mixed and liquid phases. Between UTC 02:28:20 – 02:31:40, ice particles coexist with supercooled liquid water. This heterogeneous segment is identified as mixed phase by CAM5 and E3SM but as liquid phase in CAM6. The IWC (0.01 – 10 g m^{-3}) and N_{ice} (0.01 – 0.1 cm^{-3}) in 1-s observations are underestimated in the simulations by 2 and 0.5 – 2 orders of magnitude, respectively. In the later segment UTC 02:31:20 – 02:43:20, all three models produce spurious ice particles, leading to higher glaciation ratios than the value (zero) in 1-s observations. Both CAM6 and E3SM show similar LWC and N_{liq} to observations within one order of magnitude, while CAM5 shows lower LWC and N_{liq} than observations by 1.5 and 1 orders of magnitude, respectively.

Figures 6 and 7 show an example of heterogeneously mixed ice particles and supercooled liquid water from RF03. During UTC 00:41:40 – 00:52:30, temperatures remain relatively constant at -3°C, while RH_{liq} varies between 90% and 105% (Figure 6 a), which partly contributes to the heterogeneous distributions of clear-sky conditions and three cloud phases. Cloud imageries of the Fast-2DC probe verify the identification of three cloud phases (Figure 6 d – f). Both CAM models show the same results as they mainly identify mixed phase only. In contrast, E3SM mainly identifies ice phase only. All simulated temperatures are within 1°C around the observed values. Simulated RH_{liq} are almost identical in CAM6 and CAM5 at liquid saturation, while E3SM shows RH_{liq} at 95% – 97%, which leads to a less favorable condition of supercooled liquid water and likely causes the missing LWC in E3SM. Consistent with results from RF04 and RF03, all three models underestimate IWC by 1 – 2 orders of magnitude compared with 1-s observations, while LWC simulated by CAM6 is the most similar to the observed values. During UTC 00:47:30 – 00:52:40, the 1-Hz observations show glaciation ratio mostly at one, but CAM5 and CAM6 show

glaciation ratio around 0.6 and 0.2, respectively, due to the underestimation of IWC. Even though E3SM shows a glaciation ratio at one for this segment, it is due to the combined effects of underestimating IWC and missing LWC.

3.2 Cloud phase occurrence frequency and distributions of LWC, IWC and glaciation ratio

Cloud phase occurrence frequencies for the entire SOCRATES campaign are compared with model simulations (Figure 8). The number of samples for three cloud phases is shown in the supplementary Figure S1. Figure 8 b and c show the cloud phase occurrence frequencies for 200 s and 580 s spatially averaged observation (horizontal scales of 35 and 100 km, respectively). An increase in spatial scale also increases the occurrence frequencies of mixed phase between -35°C to 0°C by a factor of 2 – 4, i.e., mixed phase frequencies are 0.05 – 0.1 for 1-s observations, compared with 0.1 – 0.3 for 200-s and 0.1 – 0.4 for 580-s observations. The increase of mixed phase frequency is compensated by the reduction of liquid and ice phase frequency above and below -20°C, respectively.

Simulations are further examined with two types of simulated IWC – one contains both ice crystals and snow (Figure 8 d – f) which is used as the default definition of simulated LWC, while the other contains only ice crystals (g – i). Excluding snow as part of the simulated IWC increases (decreases) liquid (mixed) phase frequency by 0.1 – 0.2 in three simulations. Compared with the 580-s observations, CAM6 (Figure 8 d) shows the most similar cloud phase frequencies for ice, liquid, and mixed phases. The minor issue with CAM6 is slightly lower (higher) mixed (liquid) phase frequency by 0.1 at -20ºC to 0 ºC than 580-s averaged observations. CAM6 significantly improves the presence of supercooled liquid water below -10°C compared with CAM5, which shows zero frequency of liquid-containing clouds below -10°C. The lack of supercooled liquid

373 water below -10°C in CAM5 was also shown in the previous work of D'Alessandro et al. (2019).
374 E3SM (Figure 8 f) underestimates (overestimates) the frequency of ice phase clouds below (above)
375 -20°C by 0.1 compared with 580-s averaged observations. E3SM was found to overestimate of
376 liquid cloud fraction between -20°C and -30°C at high latitudes (Y. Zhang et al., 2019). It was also
377 found to underestimate pure ice clouds at most temperatures except for close to -40°C based on a
378 global-scale evaluation (Rasch et al., 2019). A similar result of E3SM overestimating supercooled
379 liquid water below -20°C was also documented in Zhang et al. (2020) for an analysis of Arctic
380 clouds.

381 Effects of spatial scales are examined in Figure 9 a – c for observations that are spatially
382 averaged by every 10 s, 50 s, 100 s, 200 s, 290 s, and 580 s, which represent horizontal scales of
383 1.7, 8.6, 17, 35, 50 and 100 km, respectively. The overall trend of an increasing liquid (ice) phase
384 frequency in a warmer (colder) environment remains unchanged. Larger spatial scales consistently
385 show increase in the occurrence frequencies of mixed phase between -35°C to 0°C. Furthermore,
386 length scales of three cloud phases in 1-Hz observations are examined in Figure 9 d – f. The
387 number of samples for Figure 9 is shown in supplementary Figure S2. Length scales of individual
388 cloud phase segments are calculated by the consecutive seconds of the same cloud phase in 1-Hz
389 observations. The shorter and longer length scales represent more heterogeneous and
390 homogeneous distributions of cloud phases, respectively. The observations show more mixed
391 phase segments at shorter length scales (1–3 seconds) than longer length scales (> 10 seconds),
392 while the liquid and ice phases dominate the longer length scales (> 10 seconds). This result
393 indicates that the coexistence of ice and liquid occurs more frequently at shorter length scales,
394 likely due to the effective transition from liquid to ice via the WBF process.

Cloud microphysical properties, i.e., LWC, IWC, and glaciation ratios are examined for various temperatures (binned by 5°C) in Figure 10. The number of samples for this analysis is shown in supplementary Figure S3. 1-s, 200-s, and 580-s averaged observations are compared with model simulations. Averaging observations over 200 seconds significantly reduces the average LWC and IWC by 1 – 2 orders of magnitude compared with 1-s data, while the 580-s averaged observations show further reduction of LWC and IWC by up to 0.5 order of magnitude. Compared with 580-s averaged observations, CAM6 (E3SM) shows similar average LWC to the observations above -5ºC (-15ºC) but lower average LWC at lower temperatures by 0.5 – 2 orders of magnitude. Consistent with Figure 8, CAM5 lacks LWC below -10ºC. For the average IWC, all three models underestimate IWC by 1 – 2, 0.5 – 1.5, and 0.5 – 1 orders of magnitude compared with 1-s, 200-s, and 580-s observations, respectively.

Two types of glaciation ratios are calculated, one is for all in-cloud conditions (Figure 10 g – i), and the other one for conditions with coexisting ice particles and supercooled liquid water only (j – l). For the former type, the glaciation ratios are controlled by the ratios between ice phase and liquid phase occurrence frequencies, the two dominant phases. For the latter type, the glaciation ratios are controlled by the mass partitioning between ice and liquid when they coexist. For the former type of glaciation ratios, observations and CAM6 show similar results (Figure 10 g), consistent with their similar cloud phase frequencies in Figure 8. The latter glaciation ratios in CAM6 (Figure 10 j) are significantly lower than the 580-s averaged observations by 0.3 – 0.8, due to the underestimation of IWC in the model. E3SM overestimates the former type of glaciation ratios above -20°C, and underestimates the latter type of glaciation ratios below -20°C. These analyses show that even though CAM6 produces glaciation ratios of all in-cloud conditions very

similar to the observations, its underestimation of IWC leads to large biases of mass partitioning inside the mixture of ice and liquid.

A similar analysis to Figure 10 is done using simulated IWC containing only ice crystals (supplementary Figure S4). When excluding snow in the simulated IWC, even larger model biases of IWC by a factor of 2 – 3 are seen compared with including snow in the simulated IWC. Additionally, a sensitivity test is conducted to examine the impacts of model output frequency, by using E3SM output that is closest to every 1 second, 1 minute, and 10 minutes of observations (supplementary Figure S5). The results show very similar results for cloud phase frequencies, average LWC, IWC and glaciation ratios under various model output frequencies.

3.3 Thermodynamic conditions for clear-sky, in-cloud conditions and three cloud phases

Thermodynamic conditions are crucial for the formation of ice particles and supercooled liquid water, as illustrated in the case studies in Section 3.1. Figure 11 shows probability density functions (PDFs) of temperature and RH_{ice} categorized by in-cloud and clear-sky conditions (top two rows) and three cloud phases (bottom two rows). The PDF is calculated as the number of samples of a certain condition (such as in-cloud) at each bin divided by the total number of samples of that condition in all bins. PDFs of temperatures are comparable between observations and simulations. PDFs of RH_{ice} for in-cloud conditions in the simulations show lower maximum values (CAM6 134%, CAM5 116%, E3SM 144%) compared with 1-s observations (147%), but the simulated values of CAM6 and CAM5 are closer to 580-s averaged observations (127%). Similarly, PDFs of RH_{ice} for clear-sky conditions in the simulations show lower maximum values (CAM6 111%, CAM5 104%, E3SM 125%) than 1-s observations (142%) but are closer to 580-s averaged observations (109%). The simulations also underestimate the frequencies of sub-saturated

conditions for in-cloud RH_{ice}, since the 1-s and 580-s averaged observations show minimum in-cloud RH_{ice} at 4% and 8%, respectively, while simulations show minimum values of 25% – 66%.

In terms of PDFs of RH_{ice} in three cloud phases, the peak positions of RH_{ice} in 1-s observations are located around 100% – 102% for all three phases. For 580-s observations, the peak positions are located at lower values (~90%) due to the inclusion of clear-sky segments in the averaging process. Three simulations show peaks of in-cloud RH_{ice} around 100%, but with narrower ranges for all three cloud phases. For both observations and simulations, mixed phase is associated with a narrower RH_{ice} range than ice and liquid phases, consistent with the theoretical condition for WBF process with $e_{s,ice} < e < e_{s,liq}$. The lack of sub-saturated conditions for ice phase may contribute to the underestimation of ice growth and the riming effect during sedimentation, which possibly leads to lower IWC in the simulations.

3.4. Aerosol indirect effects on cloud microphysical properties

In this section, aerosol indirect effects on cloud microphysical properties at various temperatures are examined based on the relationships between total aerosol number concentrations (Na) and cloud microphysical properties (Figures 12 – 14). Since CAM5 significantly underestimates the amount of supercooled liquid water below -10°C, the model evaluation in this section focuses on CAM6 and E3SM only. The number of samples related to these figures is shown in supplementary Figures S6 and S7. The analysis is based on Na separated into two groups – aerosols with diameters > 500 nm (hereafter named as Na_{500}) and > 100 nm (named as Na_{100}). Previously, DeMott et al. (2010) showed that at temperatures higher than -36°C, Na_{500} is well correlated with number concentrations of INPs, which can facilitate ice crystal formation during heterogeneous nucleation.

For the impacts of larger aerosols, as $\log_{10}(Na_{500})$ increases, the 1-Hz observations show increasing LWC and N_{liq} between -18°C and 0°C, and increasing IWC and N_{ice} between -35°C and 0°C (Figure 12), indicating Twomey effects on both liquid droplets and ice particles at these temperature ranges. Similar effects are also present in the 580-s observations, indicating that these aerosol indirect effects are consistently observed from horizontal scales of hundreds of meters to 100 kilometers. Between -25°C and -18°C, higher Na_{500} values were observed (> 1000 cm^{-3}). A significant increase of IWC (up to 10 g m^{-3}) and N_{ice} (up to 0.1 cm^{-3}) are seen at higher Na_{500} values at this temperature range, starting from Na_{500} as low as 3 cm^{-3}. This feature indicates a possible existence of effective INPs at this level, while future work is warranted to investigate the origins of these larger aerosols. LWC and N_{liq} at this level are also lower than those at temperatures above -18ºC, possibly due to more effective evaporation of liquid droplets via the WBF process when more ice particles exist.

The analysis of Na_{100} (Figure 13) shows similar results to Na_{500}, that is, as Na_{100} increases, increasing IWC and N_{ice} are seen from -35°C to 0°C with a strong increase between -25°C and -18°C. On the other hand, LWC and N_{liq} increase with increasing Na_{100} from -18°C to 0°C, and the LWC and N_{liq} at -25°C to -18°C are lower than those at -18°C to 0°C by 2 orders of magnitude.

In terms of model simulations, both CAM6 and E3SM capture the decreasing trend of maximum Na_{500} and Na_{100} as temperature decreases, yet the maximum values of simulated Na_{500} and Na_{100} are 10 and 100 cm^{-3}, respectively, which are 2 orders of magnitude smaller than the 580-s observations. For aerosol indirect effects on liquid droplets, CAM6 and E3SM show smaller increases of LWC and N_{liq} when Na_{500} and Na_{100} increase between -15°C and 0°C. That is, the 580-s observations show LWC and N_{liq} increase 2 – 3 orders of magnitude when Na_{500} increases

484 from 0.01 cm^{-3} to 3.2 cm^{-3}, while LWC and N_{liq} increase 1 (0.5) order of magnitude in CAM6
485 (E3SM). For aerosol indirect effects on ice particles, E3SM shows increases of N_{ice} by 1 – 2 orders
486 of magnitude when Na_{500} increases from 0.01 cm^{-3} to 3.2 cm^{-3} at a narrow temperature range
487 between -20°C and -10°C, smaller than the increases seen in the observations (~2 orders of
488 magnitude). Almost no effects on IWC are seen in CAM6 or E3SM. Overall, these results indicate
489 that the models underestimate aerosol indirect effects on both liquid droplets and ice particles.

490 Aerosol indirect effects on phase partitioning and cloud fraction are examined in Figure 14.
491 Two types of glaciation ratios are examined – for all in-cloud condition (a–h) and coexisting ice
492 and liquid only (i–p). For the glaciation ratios of all in-cloud conditions, the observations show
493 both temperature effect and aerosol indirect effect, that is, glaciation ratios increase with
494 decreasing temperature as well as with increasing Na_{500} and Na_{100}. When larger aerosols exist,
495 observations show that glaciation ratios mostly reach unity below -20°C (Figure 14 a and b). The
496 significant increase of glaciation ratios with increasing Na_{500} and Na_{100} at -25°C – -18°C is
497 consistent with the large increase of IWC in Figures 12 and 13. At temperature above -18°C,
498 increase of glaciation ratio is also observed at higher Na. The second type of glaciation ratios for
499 coexisting ice and liquid also shows an increasing trend with increasing Na_{500} and Na_{100}, although
500 fewer samples are seen at unity than the first type of glaciation ratios. This indicates that the phase
501 partitioning within the mixture of ice and liquid is less affected by Na, but the phase partitioning
502 among all three cloud phases is affected by Na more strongly.

503 For both CAM6 and E3SM, only temperature effect is seen and no aerosol indirect effects
504 are seen on either type of glaciation ratios, which is consistent with the lack of aerosol indirect
505 effects on ice particles in Figures 12 and 13. Cloud fraction is calculated by normalizing the
506 number of in-cloud samples in each bin by the total number of samples in that bin. Note that the

cloud fraction for simulations is not based on the model output "cloud fraction", but rather is calculated based on the in-cloud definition described in Section 2.3. 100% cloudiness is seen in 1-s (580-s) observations at Na_{500} > 3 cm^{-3} (> 0.1 cm^{-3}) and Na_{100} > 300 cm^{-3} (> 100 cm^{-3}). Both CAM6 and E3SM show a slight increase of cloud fraction from below to above -15°C, yet no clear relationship between cloud fraction and aerosol concentrations is seen.

4. Conclusions and Implications to Model Development

This study focuses on examining cloud characteristics at -40°C to 0°C over the Southern Ocean based on in situ aircraft-based observations and three GCM simulations (i.e., CAM6, CAM5, and E3SM). A series of cloud characteristics are examined, including cloud phases, mass and number concentrations of cloud hydrometeors, phase partitioning, thermodynamic conditions, and aerosol indirect effects. Several approaches are used to facilitate the comparison between in situ observations and GCM simulations, including using nudged simulations toward reanalysis data, recalculating cloud properties based on instrument measurement ranges, and examining the impacts of spatial scales on the comparison results.

Spatially averaging observation data from 1 s to 580 s (i.e., from ~0.2 – 100 km in horizontal) is found to affect several variables, such as reducing average LWC and IWC by 1 – 2 orders of magnitude due to the inclusion of clear-sky segments in the grid-mean averages, increasing the occurrence frequency of mixed phase clouds since ice particles and supercooled liquid water are more likely to coexist at coarser scales, reducing the maximum RH_{ice} for in-cloud and clear-sky conditions, and decreasing the peak positions of RH_{ice} PDFs for three cloud phases. For other characteristics, spatial averaging has a small impact on the average glaciation ratios of

all in-cloud conditions, and the positive correlations of LWC, IWC, N_{liq}, and N_{ice} with respect to aerosol number concentrations.

Evaluation of three model simulations shows that CAM6 has the most similar cloud phase occurrence frequency to observations compared with CAM5 and E3SM. Particularly, CAM6 and E3SM significantly improve the proportion of liquid and mixed phase clouds below -10°C compared with the CAM5. This is most likely due to the removal of a temperature-dependent mass partitioning function between ice and liquid in the shallow convection scheme (Park & Bretherton, 2009) that was previously used in CAM5, as discussed in previous studies (Gettelman et al., 2020; Kay et al., 2016). E3SM underestimates (overestimates) ice phase frequencies below (above) -20°C. When evaluating simulated LWC compared with 580-s observations, CAM6 and E3SM overestimate LWC values by 0.5 – 2 orders of magnitude below -5ºC and -15ºC, respectively. Another main model bias is the underestimation of IWC at all temperatures between -40°C and 0°C by 0.5 – 1 orders of magnitude compared with 580-s observations. Even though CAM6 shows small biases of glaciation ratios of all in-cloud conditions (i.e., with biases less than ±0.1), it significantly underestimates glaciation ratios of coexisting ice and liquid by 0.3 – 0.8 due to the underestimation of IWC.

Thermodynamic conditions, specifically RH, are found to be well correlated with model biases of cloud occurrences and cloud phases as illustrated in case studies. This result combined with the previous study (Wu et al., 2017) which showed that RH biases in the CAM5 are dominated water vapor biases indicates that the representation of water vapor distribution is important for simulating clouds over the Southern Ocean. In terms of PDFs of in-cloud RH_{ice}, 1-s observations show larger variabilities of in-cloud RH_{ice} ranging from 4% to 147%, while the simulations show narrower ranges, i.e., 25%–134% for CAM6, 52%–116% for CAM5, and 66%–144% for E3SM.

When averaging the observations into every 580 s, the observed in-cloud RH_{ice} is seen from 8% to 127%, indicating that the simulations lack of sub-saturation at in-cloud conditions . This may limit the ranges of cloud microphysical properties, such as underestimating IWC by limiting ice growth and riming in sub-saturated conditions.

Regarding aerosol indirect effects on cloud microphysical properties, positive correlations are found between cloud microphysical properties (IWC, LWC, N_{ice}, and N_{liq}) and the number concentration of larger and smaller aerosols (i.e., Na_{500} and Na_{100}, respectively), suggesting the Twomey effect on ice particles at -35°C to 0°C, and on supercooled liquid water from -18°C to 0°C. The increase of LWC and N_{liq} with increasing Na are stronger at warmer conditions (-18°C to 0°C), possibly due to less activation of ice nucleation at this temperature range and therefore less reduction of LWC and N_{liq} due to the WBF process. On the other hand, aerosol indirect effects on IWC and N_{ice} are stronger at -25°C – -18°C, indicating possible effective INPs at this vertical level. Higher glaciation ratios of all in-cloud conditions are also found to be associated with higher Na and lower temperatures in both 1-s and 580-s observations. Small increases of LWC and N_{liq} with increasing Na are seen in CAM6 and E3SM between -15°C to 0°C, yet the models miss the increasing IWC and N_{ice} with increasing Na at -25°C to -18°C. Small increases of N_{ice} are seen in E3SM only at a narrow temperature range (-20°C to -10°C), while no obvious aerosol indirect effects are seen on IWC, cloud fraction or either type of glaciation ratios in CAM6 and E3SM. These results suggest that stronger aerosol indirect effects on both liquid droplets and ice particles should be considered for future development of cloud microphysics parameterizations, especially since model parameterizations still have limited aerosol types acting as INPs. In addition, the maximum Na_{500} and Na_{100} values are underestimated in CAM6 and E3SM by 1 – 2 orders of magnitude compared with 580-s observations, suggesting that higher concentrations of INPs and

cloud condensation nuclei (CCN) need to be included in the model. In fact, higher CCN number concentration has also been recommended in another model evaluation study on CAM6 by Gettelman et al. (2020).

Overall, this study provides a series of metrics for model evaluation of ice, liquid, and mixed phase clouds at -40°C to 0°C based on high resolution, in situ observations. Both thermodynamic conditions and aerosol number concentrations are found to be important factors in controlling cloud phases, the mass partition of ice and liquid, and cloud hydrometeor mass and number concentrations. The model evaluation in this study is restricted to default configurations of three GCMs, while future work is warranted to investigate the impacts of individual parameters in cloud microphysics parameterizations that may lead to improved results compared with observations. The observation-based statistical distributions of cloud phase frequency, microphysical properties, and their correlations with temperature, RH, and aerosol concentrations can be used to guide future model development at various horizontal scales.

Acknowledgement

C. Yang and M. Diao acknowledge funding from the NSF Division of Atmospheric and Geospace Sciences (AGS) grant #1642291 and NSF Office of Polar Programs (OPP) grant #1744965. M. Diao also acknowledges funding from the Department of Energy (DOE) Atmospheric System Research (ASR) grant DE-SC0021211, and the support of the NCAR Advanced Study Program (ASP) Faculty Fellowship in 2016 and 2018. C. Yang received the Walker Fellowship from San Jose State University. A. Gettelman acknowledges funding from the NSF OPP grant #1744946. K. Zhang and J. Sun acknowledges support from the Energy Exascale Earth System Model project. The Pacific Northwest National Laboratory is operated for the U.S. DOE by Battelle Memorial

Institute under contract DE-AC05-76RL01830. We acknowledge the support from the NCAR/Earth Observing Laboratory pilots, technicians, and flight crews for the NSF SOCRATES flight campaign. NCAR is sponsored by the National Science Foundation. M. Diao provided laboratory calibrations and QA/QC of the VCSEL hygrometer and S. Beaton contributed to the field support. All aircraft observations can be obtained at https://data.eol.ucar.edu/.

References

Bergeron, T. (1928). Über die dreidimensional verknüpfende Wetteranalyse. *Geophys. Norv.*, *5*(7), 1–111. https://doi.org/10.1175/1520-0493(1931)59<275:TBBDDV>2.0.CO;2

Bodas-Salcedo, A., Hill, P. G., Furtado, K., Williams, K. D., Field, P. R., Manners, J. C., et al. (2016). Large Contribution of Supercooled Liquid Clouds to the Solar Radiation Budget of the Southern Ocean. *J. Climate*, *29*, 4213–4228. https://doi.org/10.1175/JCLI-D-15-0564.1

Borys, R. D., Lowenthal, D. H., Cohn, S. A., & Brown, W. O. J. (2003). Mountaintop and radar measurements of anthropogenic aerosol effects on snow growth and snowfall rate. *Geophysical Research Letters*, *30*(10). https://doi.org/10.1029/2002gl016855

Bühl, J., Seifert, P., Engelmann, R., & Ansmann, A. (2019). Impact of vertical air motions on ice formation rate in mixed-phase cloud layers. *npj Clim Atmos Sci*, *2*(36) https://doi.org/10.1038/s41612-019-0092-6

Chen, T., Rossow, W. B., & Zhang, Y. (2000). Radiative Effects of Cloud-Type Variations. *J. Climate*, *13*(264–286). https://doi.org/10.1175/1520-0442(2000)013<0264:REOCTV>2.0.CO;2

D'Alessandro, J. J., Diao, M., Wu, C., Liu, X., Jensen, J. B., & Stephens, B. B. (2019). Cloud phase and relative humidity distributions over the Southern Ocean in austral summer based on in situ observations and CAM5 simulations. *Journal of Climate*, *32*(10), 2781–2805. https://doi.org/10.1175/JCLI-D-18-0232.1

DeMott, P. J., Prenni, A. J., Liu, X., Kreidenweis, S. M., Petters, M. D., Twohy, C. H., et al. (2010). Predicting global atmospheric ice nuclei distributions and their impacts on climate. *Proceedings of the National Academy of Sciences of the United States of America*, *107*(25), 11217–11222. https://doi.org/10.1073/pnas.0910818107

Diao, M. (2020). VCSEL 1 Hz Water Vapor Data. *UCAR/NCAR - Earth Observing Laboratory*. https://doi.org/10.26023/KFSD-Y8DQ-YC0D, https://data.eol.ucar.edu/dataset/552.051

Eidhammer, T., Morrison, H., Bansemer, A., Gettelman, A., & Heymsfield, A. J. (2014). Comparison of ice cloud properties simulated by the Community Atmosphere Model (CAM5) with in-situ observations. *Atmos. Chem. Phys*, *14*, 10103–10118. https://doi.org/10.5194/acp-14-10103-2014

Fan, J., Ghan, S., Ovchinnikov, M., Liu, X., Rasch, P. J., & Korolev, A. (2011). Representation of Arctic mixed-phase clouds and the Wegener-Bergeron-Findeisen process in climate models: Perspectives from a cloud-resolving study. *Journal of Geophysical Research*, *116*(D00T07). https://doi.org/10.1029/2010JD015375

Gettelman, A., & Morrison, H. (2015). Advanced two-moment bulk microphysics for global models. Part I: Off-line tests and comparison with other schemes. *Journal of Climate*, *28*(3), 1268–1287. https://doi.org/10.1175/JCLI-D-14-00102.1

Gettelman, A., Bardeen, C., McCluskey, C. S., Järvinen, E. J, Stith, J., Brethenton, C., McFarquhar, G., Twohy, C., D'Alessandro, J., & Wu, W. (2020) Simulating Observations of Southern Ocean Clouds and Implications for Climate. *Journal of Geophysical Research*. In press.

Gierens, R., Kneifel, S., Shupe, M. D., Ebell, K., Maturilli, M., & Löhnert, U. (2020). Low-level mixed-phase clouds in a complex Arctic environment. *Atmospheric Chemistry and Physics*, *20*(6), 3459–3481. https://doi.org/10.5194/acp-20-3459-2020

Guo, Z., Wang, M., Peng, Y., & Luo, Y. (2020). Evaluation on the Vertical Distribution of Liquid and Ice Phase Cloud Fraction in Community Atmosphere Model Version 5.3 using Spaceborne Lidar Observations. *Earth and Space Science*, *7*, e2019EA001029, https://doi.org/10.1029/2019EA001029

Hallett, J., & Mossop, S. C. (1974). Production of secondary ice particles during the riming process. *Nature*, *249*(5452), 26–28. https://doi.org/10.1038/249026a0

Jackson, R. C., McFarquhar, G. M., Korolev, A. V., Earle, M. E., Liu, P. S. K., Lawson, R. P., et al. (2012). The dependence of ice microphysics on aerosol concentration in arctic mixed-phase stratus clouds during ISDAC and M-PACE. *Journal of Geophysical Research: Atmospheres*, *117*, D15207, https://doi.org/10.1029/2012JD017668

Kay, J. E., Hillman, B. R., Klein, S. A., Zhang, Y., Medeiros, B., Pincus, R., et al. (2012). Exposing Global Cloud Biases in the Community Atmosphere Model (CAM) Using Satellite Observations and Their Corresponding Instrument Simulators. *J. Climate*, *25*(15), 5190–5207. https://doi.org/10.1175/JCLI-D-11-00469.1

Kay, J. E., Wall, C., Yettella, V., Medeiros, B., Hannay, C., Caldwell, P., & Bitz, C. (2016). Global Climate Impacts of Fixing the Southern Ocean Shortwave Radiation Bias in the Community Earth System Model (CESM). *Journal of Climate*, *29*(12), 4617–4636. https://doi.org/10.1175/JCLI-D-15-0358.1

662 Klein, S. A., Mccoy, R. B., Morrison, H., Ackerman, A. S., Avramov, A., De Boer, G., et al.
663 (2009). Intercomparison of model simulations of mixed-phase clouds observed during the
664 ARM Mixed-Phase Arctic Cloud Experiment. I: Single-layer cloud. *Q. J. R. Meteorol. Soc*,
665 *135*, 979–1002. https://doi.org/10.1002/qj.416

666 Korolev, A., McFarquhar, G., Field, P. R., Franklin, C., Lawson, P., Wang, Z., et al. (2017).
667 Mixed-Phase Clouds: Progress and Challenges. *Meteorological Monographs*, *58*, 5.1-5.50.
668 https://doi.org/10.1175/amsmonographs-d-17-0001.1

669 Korolev, A., & Isaac, G. (2003). Phase transformation of mixed-phase clouds. *Quarterly Journal*
670 *of the Royal Meteorological Society*, *129*(587), 19–38. https://doi.org/10.1256/qj.01.203

671 Korolev, A., & Isaac, G. A. (2006). Relative humidity in liquid, mixed-phase, and ice clouds.
672 *Journal of the Atmospheric Sciences*, *63*(11), 2865–2880.
673 https://doi.org/10.1175/JAS3784.1

674 Korolev, A., & Field, P. R. (2008). The Effect of Dynamics on Mixed-Phase Clouds: Theoretical
675 Considerations. *J. Atmos. Sci.*, 65, 66–86, https://doi.org/10.1175/2007JAS2355.1

676 Lin, S.-J. (2004). A "Vertically Lagrangian" Finite-Volume Dynamical Core for Global Models.
677 *Mon. Wea. Rev.*, *132*, 2293–2307. https://doi.org/10.1175/1520-
678 0493(2004)132<2293:AVLFDC>2.0.CO;2

679 Liou, K. N. (1992), *Radiation and Cloud Processes in the Atmosphere*, pp. 255–339, Oxford
680 Univ. Press, New York.

Liu, X., Easter, R. C., Ghan, S. J., Zaveri, R., Rasch, P., Shi, X., et al. (2012). Toward a minimal representation of aerosols in climate models: Description and evaluation in the Community Atmosphere Model CAM5. *Geoscientific Model Development*, *5*(3), 709–739. https://doi.org/10.5194/gmd-5-709-2012

Liu, X., Ma, P. L., Wang, H., Tilmes, S., Singh, B., Easter, R. C., et al. (2016). Description and evaluation of a new four-mode version of the Modal Aerosol Module (MAM4) within version 5.3 of the Community Atmosphere Model. *Geoscientific Model Development*, *9*(2), 505–522. https://doi.org/10.5194/gmd-9-505-2016

Lohmann, U., Henneberger, J., Henneberg, O., Fugal, J. P., Bühl, J., & Kanji, Z. A. (2016). Persistence of orographic mixed-phase clouds. *Geophysical Research Letters*, *43*(19), 10,512-10,519. https://doi.org/10.1002/2016GL071036

Lohmann, U. (2002). Possible Aerosol Effects on Ice Clouds via Contact Nucleation. *J. Atmos. Sci.*, *59*, 647–656, https://doi.org/10.1175/1520-0469(2001)059<0647:PAEOIC>2.0.CO;2

Matus, A. V., & L'Ecuyer, T. S. (2017). The role of cloud phase in Earth's radiation budget. *Journal of Geophysical Research: Atmospheres*, *122*(5), 2559–2578. https://doi.org/10.1002/2016JD025951

McCoy, D. T., Tan, I., Hartmann, D. L., Zelinka, M. D., & Storelvmo, T. (2016). On the relationships among cloud cover, mixed-phase partitioning, and planetary albedo in GCMs. *Journal of Advances in Modeling Earth Systems*, *8*(2), 650–668. https://doi.org/10.1002/2015MS000589

Morrison, A. E., Siems, S. T., Manton, M. J., & Nazarov, A. (2010). A modeling case study of mixed-phase clouds over the Southern Ocean and Tasmania. *Monthly Weather Review*, *138*(3), 839–862. https://doi.org/10.1175/2009MWR3011.1

Morrison, H., & Gettelman, A. (2008). A New Two-Moment Bulk Stratiform Cloud Microphysics Scheme in the Community Atmosphere Model, Version 3 (CAM3). Part I: Description and Numerical Tests. *J. Climate*, *21*(15), 3642–3659. https://doi.org/10.1175/2008JCLI2105.1

Mülmenstädt, J., Sourdeval, O., Delanoë, J., & Quaas, J. (2015). Frequency of occurrence of rain from liquid-, mixed-, and ice-phase clouds derived from A-Train satellite retrievals. *Geophysical Research Letters*, *42*(15), 6502–6509. https://doi.org/10.1002/2015GL064604

Murphy, D. M., & Koop, T. (2005). Review of the vapour pressures of ice and supercooled water for atmospheric applications. *Quarterly Journal of the Royal Meteorological Society*, *131*(608), 1539–1565. https://doi.org/10.1256/qj.04.94

Neale, R. B., Chen, C.-C., Gettelman, A., Lauritzen, P. H., Park, S., Williamson, D. L., et al. (2012). *Description of the NCAR Community Atmosphere Model (CAM 5.0)*. NCAR Tech Note TN-486, 268 pp.

Park, S., & Bretherton, C. S. (2009). The University of Washington shallow convection and moist turbulence schemes and their impact on climate simulations with the community atmosphere model. *Journal of Climate*, *22*(12), 3449–3469. https://doi.org/10.1175/2008JCLI2557.1

721 Patnaude, R., Diao, M., Liu, X., & Chu, S. (2020). Effects of Thermodynamics, Dynamics and
722 Aerosols on Cirrus Clouds Based on In Situ Observations and NCAR CAM6 Model. *Atmos.*
723 *Chem. Phys. Discuss.*, https://doi.org/10.5194/acp-2020-497

724 Qiu, S., Xi, B., & Dong, X. (2018). Influence of Wind Direction on Thermodynamic Properties
725 and Arctic Mixed-Phase Clouds in Autumn at Utqiaġvik, Alaska. *Journal of Geophysical*
726 *Research: Atmospheres*, *123*(17), 9589–9603. https://doi.org/10.1029/2018JD028631

727 Rangno, A. L., & Hobbs, P. V. (2001). Ice particles in stratiform clouds in the Arctic and
728 possible mechanisms for the production of high ice concentrations. *Journal of Geophysical*
729 *Research: Atmospheres*, *106*(D14), 15065–15075. https://doi.org/10.1029/2000JD900286

730 Rasch, P. J., Xie, S., Ma, P. -L., Lin, W., Wang, H., Tang, Q., et al. (2019). An Overview of the
731 Atmospheric Component of the Energy Exascale Earth System Model. *Journal of Advances*
732 *in Modeling Earth Systems*, *11*(8), 2377–2411. https://doi.org/10.1029/2019MS001629

733 Shupe, M. D., Kollias, P., Persson, P. O. G., & McFarquhar, G. M. (2008). Vertical Motions in
734 Arctic Mixed-Phase Stratiform Clouds. *J. Atmos. Sci.*, *65*, 1304–1322,
735 https://doi.org/10.1175/2007JAS2479.1

736 Storelvmo, T., Hoose, C., & Eriksson, P. (2011). Global modeling of mixed-phase clouds: The
737 albedo and lifetime effects of aerosols. *Journal of Geophysical Research*, *116*(D5), D05207.
738 https://doi.org/10.1029/2010JD014724

739 Sun, J., Zhang, K., Wan, H., Ma, P., Tang, Q., & Zhang, S. (2019). Impact of Nudging Strategy
740 on the Climate Representativeness and Hindcast Skill of Constrained EAMv1 Simulations.
741 *Journal of Advances in Modeling Earth Systems*, *11*(12), 3911–3933.

https://doi.org/10.1029/2019MS001831

Tan, I., & Storelvmo, T. (2016). Sensitivity study on the influence of cloud microphysical parameters on mixed-phase cloud thermodynamic phase partitioning in CAM5. *Journal of the Atmospheric Sciences*, *73*(2), 709–728. https://doi.org/10.1175/JAS-D-15-0152.1

Tan, I., Storelvmo, T., & Zelinka, M. D. (2016). Observational constraints on mixed-phase clouds imply higher climate sensitivity. Science, *352*, 224–227, https://doi.org/10.1126/science.aad5300

Trenberth, K. E., & Fasullo, J. T. (2010). Simulation of present-day and twenty-first-century energy budgets of the southern oceans. *Journal of Climate*, *23*(2), 440–454. https://doi.org/10.1175/2009JCLI3152.1

Wegener, A. (1912). Thermodynamik der Atmosphäre. *Nature*, *90*(2237), 31–31. https://doi.org/10.1038/090031a0

Williams, K. D., Bodas-Salcedo, A., Dé Qué, M., Fermepin, S., Medeiros, B., Watanabe, M., et al. (2013). The Transpose-AMIP II Experiment and Its Application to the Understanding of Southern Ocean Cloud Biases in Climate Models. *J. Climate*, *26*, 3258–3274. https://doi.org/10.1175/JCLI-D-12-00429.1

Wu, C., Liu, X., Diao, M., Zhang, K., Gettelman, A., Lu, Z., Penner, J. E., & Lin, Z. (2017). Direct comparisons of ice cloud macro- and microphysical properties simulated by the Community Atmosphere Model version 5 with HIPPO aircraft observations. *Atmos. Chem. Phys.*, *17*, 4731–4749, https://doi.org/10.5194/acp-17-4731-2017.

762 Zhang, D., Vogelmann, A., Kollias, P., Luke, E., Yang, F., Lubin, D., & Wang, Z. (2019).
763 Comparison of Antarctic and Arctic Single-Layer Stratiform Mixed-Phase Cloud Properties
764 Using Ground-Based Remote Sensing Measurements. *Journal of Geophysical Research:*
765 *Atmospheres*, *124*(17–18), 10186–10204. https://doi.org/10.1029/2019JD030673

766 Zhang, M., Liu, X., Diao, M., D'Alessandro, J. J., Wang, Y., Wu, C., et al. (2019). Impacts of
767 Representing Heterogeneous Distribution of Cloud Liquid and Ice on Phase Partitioning of
768 Arctic Mixed-Phase Clouds with NCAR CAM5. *Journal of Geophysical Research:*
769 *Atmospheres*, *124*(23), 13071–13090. https://doi.org/10.1029/2019JD030502

770 Zhang, Y., Xie, S., Lin, W., Klein, S. A., Zelinka, M., Ma, P., et al. (2019). Evaluation of Clouds
771 in Version 1 of the E3SM Atmosphere Model With Satellite Simulators. *Journal of*
772 *Advances in Modeling Earth Systems*, *11*(5), 1253–1268.
773 https://doi.org/10.1029/2018MS001562

774 Zhang, M., Xie, S., Liu, X., Lin, W., Zhang, K., Ma, H., et al. (2020). Toward Understanding the
775 Simulated Phase Partitioning of Arctic Single-Layer Mixed-Phase Clouds in E3SM. *Earth*
776 *and Space Science*, *7*(7). https://doi.org/10.1029/2020ea001125

777 Zondlo, M. A., Paige, M. E., Massick, S. M., & Silver, J. A. (2010). Vertical cavity laser
778 hygrometer for the National Science Foundation Gulfstream-V aircraft. *Journal of*
779 *Geophysical Research*, *115*(D20), D20309. https://doi.org/10.1029/2010JD014445

780

781 Table 1. The maximum and minimum values of thermodynamic conditions and cloud
782 microphysical properties used in this study for observations and simulations.

Variables	**1-s observations**	**200-s observations**	**580-s observations**	**CAM6**	**CAM5**	**E3SM**
T (°C)	-39.7 – 0.0	-39.7 – 0.0	-39.7 – 0.0	-37.6 – 0.0	-37.4 – 0.0	-38.5 – 0.0
P (Pa)	37,623 – 96,848	37,644 – 97,131	37,645 – 96,958	32,207 – 96,777	32,212 – 98,315	32,760 – 102,116
LWC (g m^{-3})	5.01×10^{-5} – 1.41	2.76×10^{-7} – 0.66	9.52×10^{-8} – 0.53	1.26×10^{-5} – 0.36	1.26×10^{-7} – 0.30	1.41×10^{-7} – 0.34
IWC (g m^{-3})	5.68×10^{-5} – 55.8	3.79×10^{-7} – 13.9	1.31×10^{-7} – 7.73	1.09×10^{-7} – 0.14	3.17×10^{-7} – 0.18	1.13×10^{-7} – 0.18
N_{liq} (cm^{-3})	4.87×10^{-5} – 564.85	2.59×10^{-7} – 218.00	9.16×10^{-8} – 210.56	5.01×10^{-4} – 86.85	1.41×10^{-7} – 185.70	1.02×10^{-7} – 85.53
N_{ice} (cm^{-3})	4.83×10^{-5} – 0.47	2.45×10^{-7} – 0.07	8.62×10^{-8} – 0.04	2.77×10^{-6} – 0.08	5.34×10^{-6} – 15.14	1.53×10^{-7} – 9.71
In-cloud RH_{liq} (%)	3.7 – 105.0	3.9 – 102.3	6.8 – 101.7	23.2 –101.3	42.3 – 99.5	55.8 – 104.5
In-cloud RH_{ice} (%)	4.3 – 146.7	4.1 – 137.3	8.0 – 126.8	25.3 – 133.8	52.1 – 115.8	65.5 – 143.8
Clear-sky RH_{liq} (%)	1.1 – 104.8	1.7 – 93.1	2.0 – 88.8	5.3 – 97.6	5.4 – 97.0	0.0 – 98.8
Clear-sky RH_{ice} (%)	1.1 – 141.8	2.0 – 117.7	2.3 – 109.2	6.3 – 110.9	6.5 – 103.6	0.0 – 125.0

783

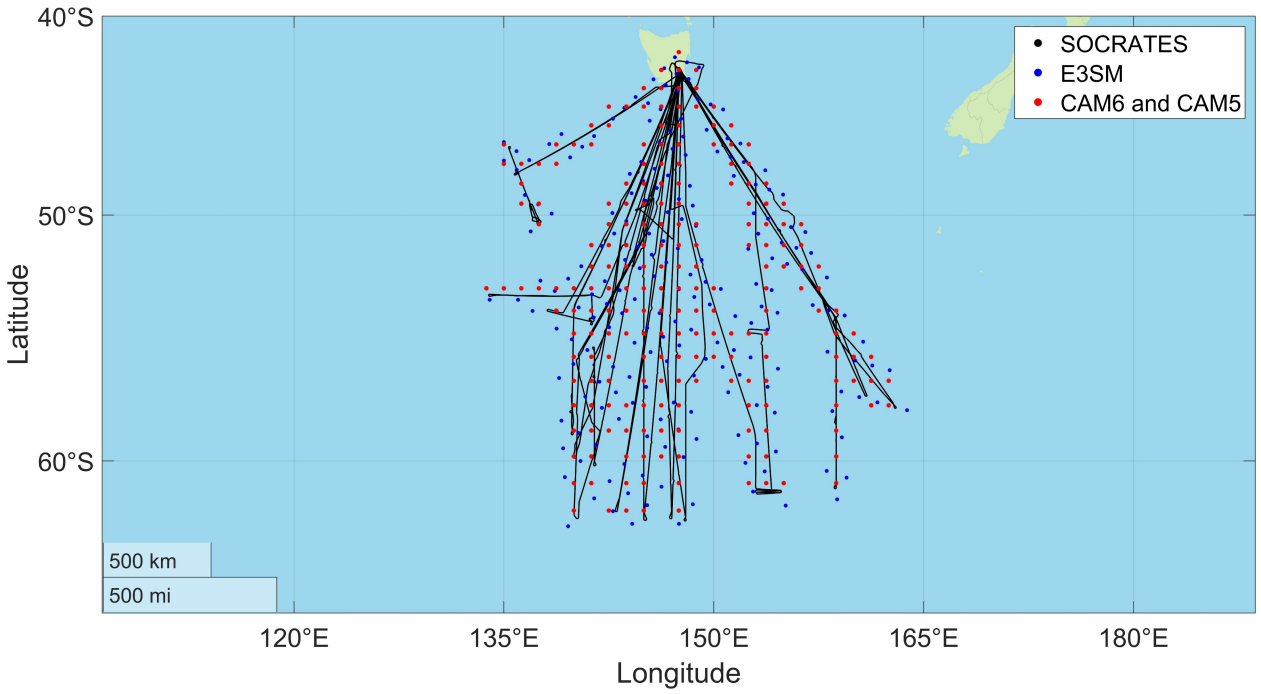

784

785 Figure 1. Flight tracks of a total 15 research flights in the NSF SOCRATES campaign (black) and

786 the collocated grid coordinates for CAM6 (red), CAM5 (red) and E3SM (blue) simulations.

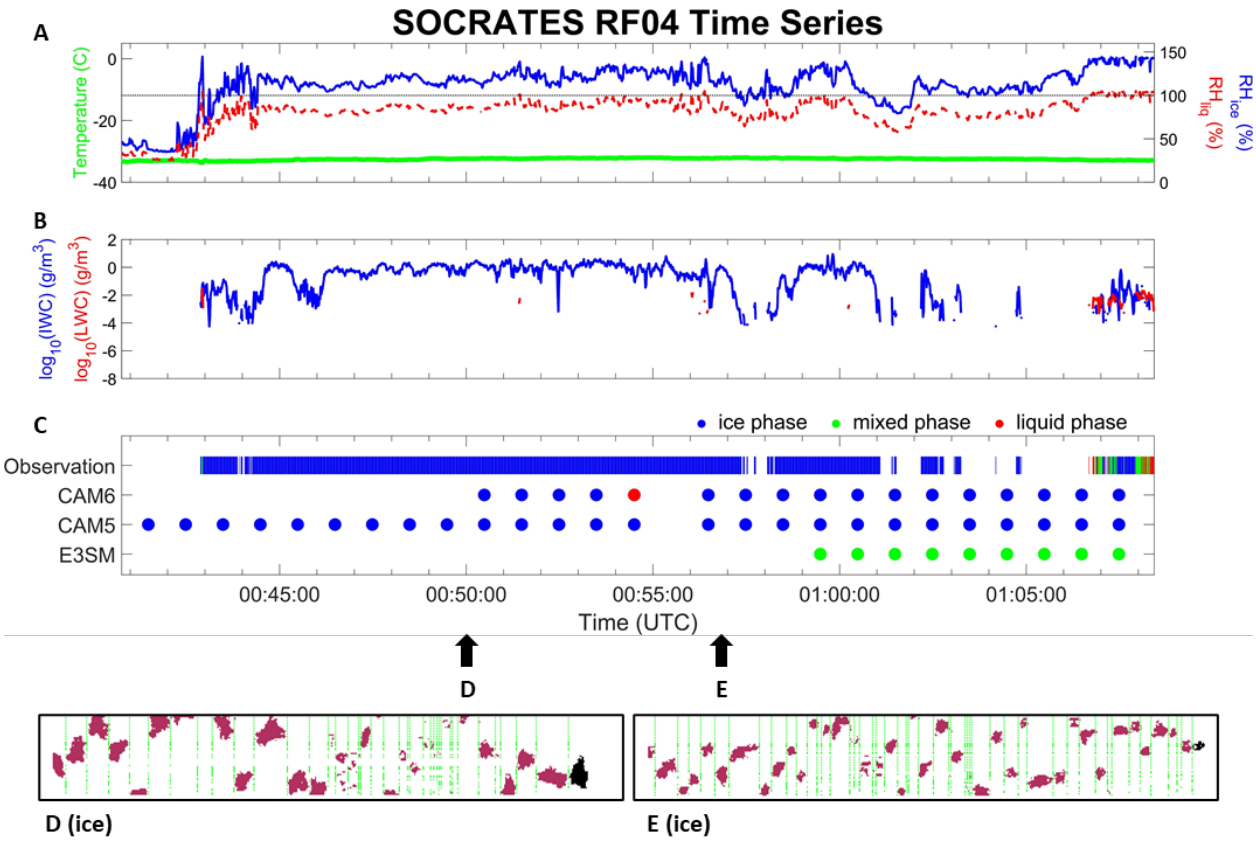

787

788 Figure 2. An example time series of ice-phase dominated clouds in NSF SOCRATES campaign
789 Research Flight 4 (RF04). (a) 1-Hz observations of temperature (green), RH_{ice} (blue), RH_{liq} (red),
790 and RH = 100% (dashed black). (b) 1-Hz observations of log-scale IWC (blue) and LWC (red). (c)
791 Cloud phases identified from the 1-Hz observations (vertical bars) and simulated by the CAM6,
792 CAM5, and E3SM (dots). (d) and (e) illustrate the seconds of ice cloud particle imageries captured
793 by the Fast-2DC probe.

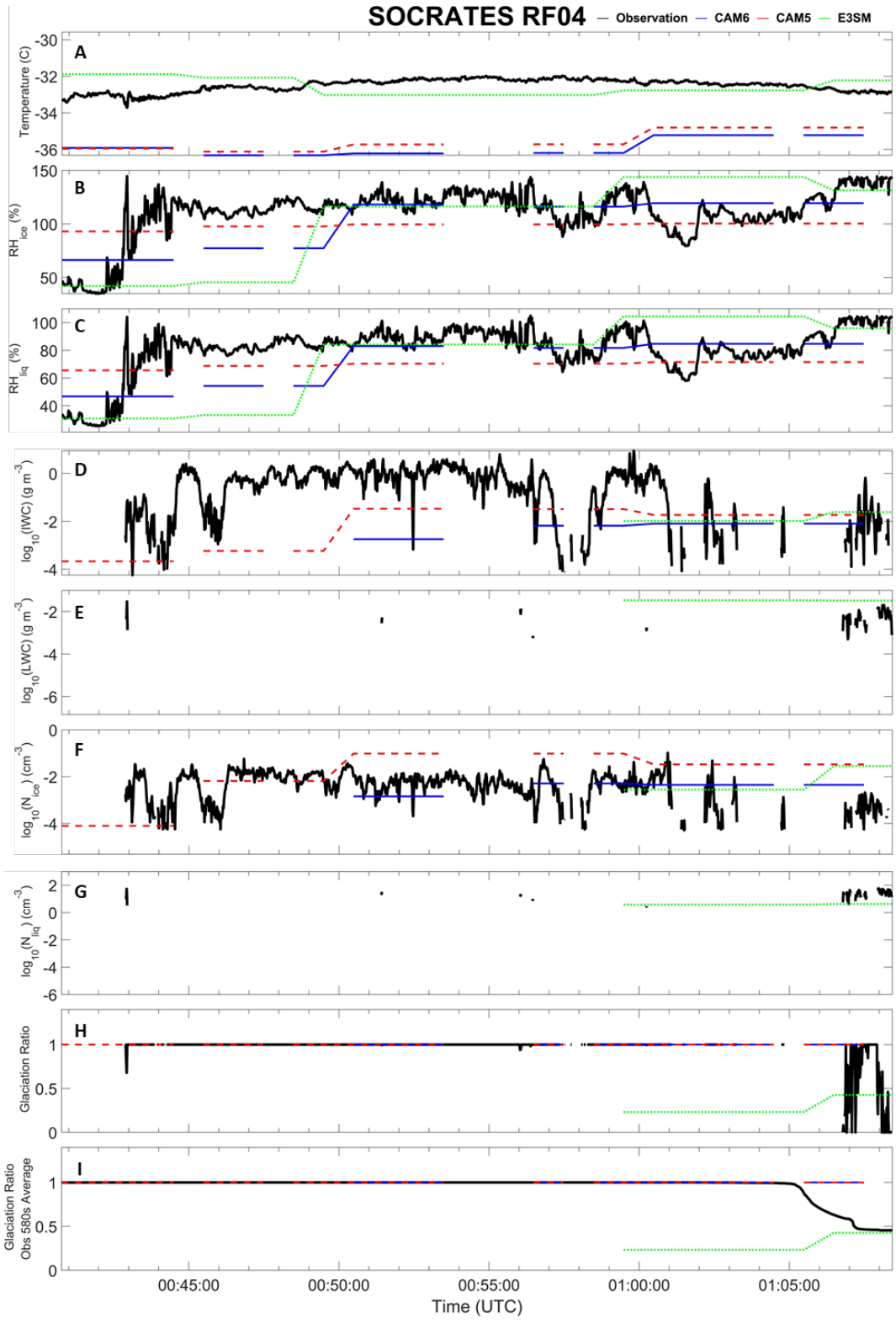

794

795 Figure 3. Time series for the same time interval of RF04 in Figure 2, compared between

796 observations and simulations, including (a) temperature, (b) RH_{ice} (c) RH_{liq}, (d) $\log_{10}$(IWC), (e)

797 $\log_{10}$(LWC), (f) N_{ice}, (g) N_{liq}, (h) glaciation ratio, and (i) glaciation ratio using 580-second
798 averaged observations. (a) to (h) are based on 1-Hz observations. Colored lines represent
799 observations (black), CAM6 (blue), CAM5 (red), and E3SM (green).

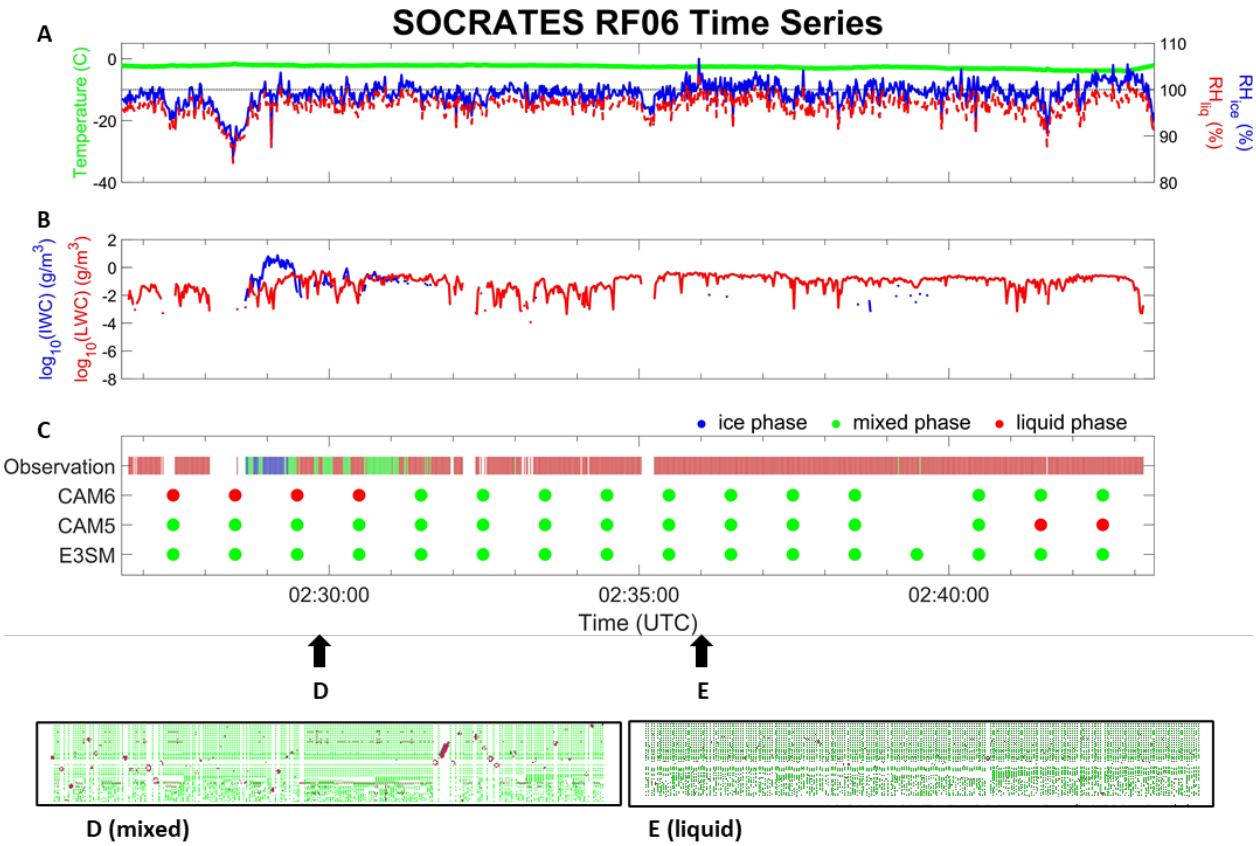

800

801 Figure 4. Similar to Figure 2 but for liquid-phase dominated clouds in Research Flight 6 (RF06).

802 In (d) and (e), individual seconds of mixed phase and liquid phase cloud particle imageries are

803 captured, respectively.

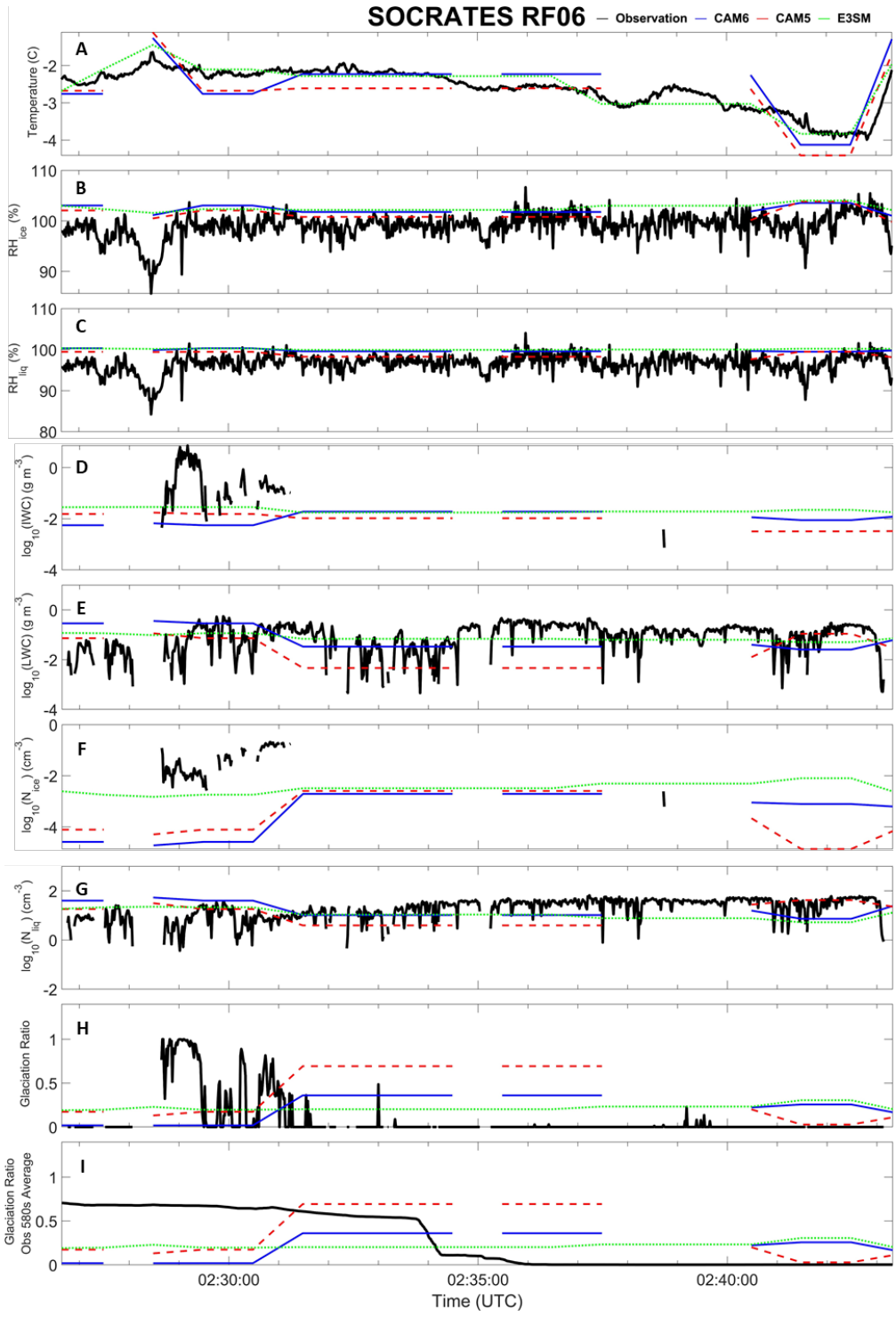

804

805 Figure 5. Similar to Figure 3 but for RF06.

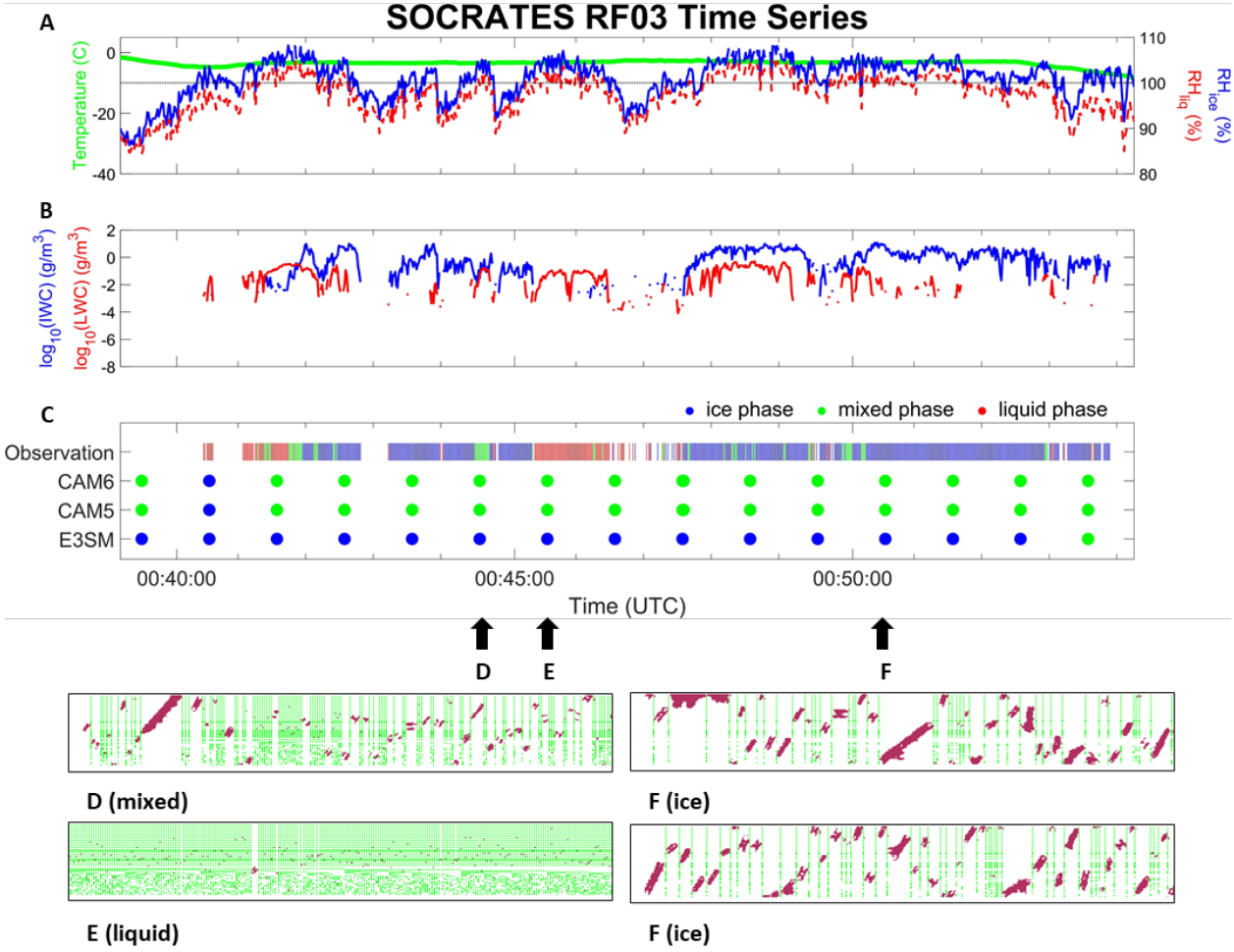

806

807 Figure 6. Similar to Figure 2 but for a case of spatially heterogeneous clouds with three phases in
808 Research Flight 3 (RF03). Individual seconds of mixed phase, liquid phase, and ice phase cloud
809 particle imageries are noted by (d), (e), and (f), respectively.

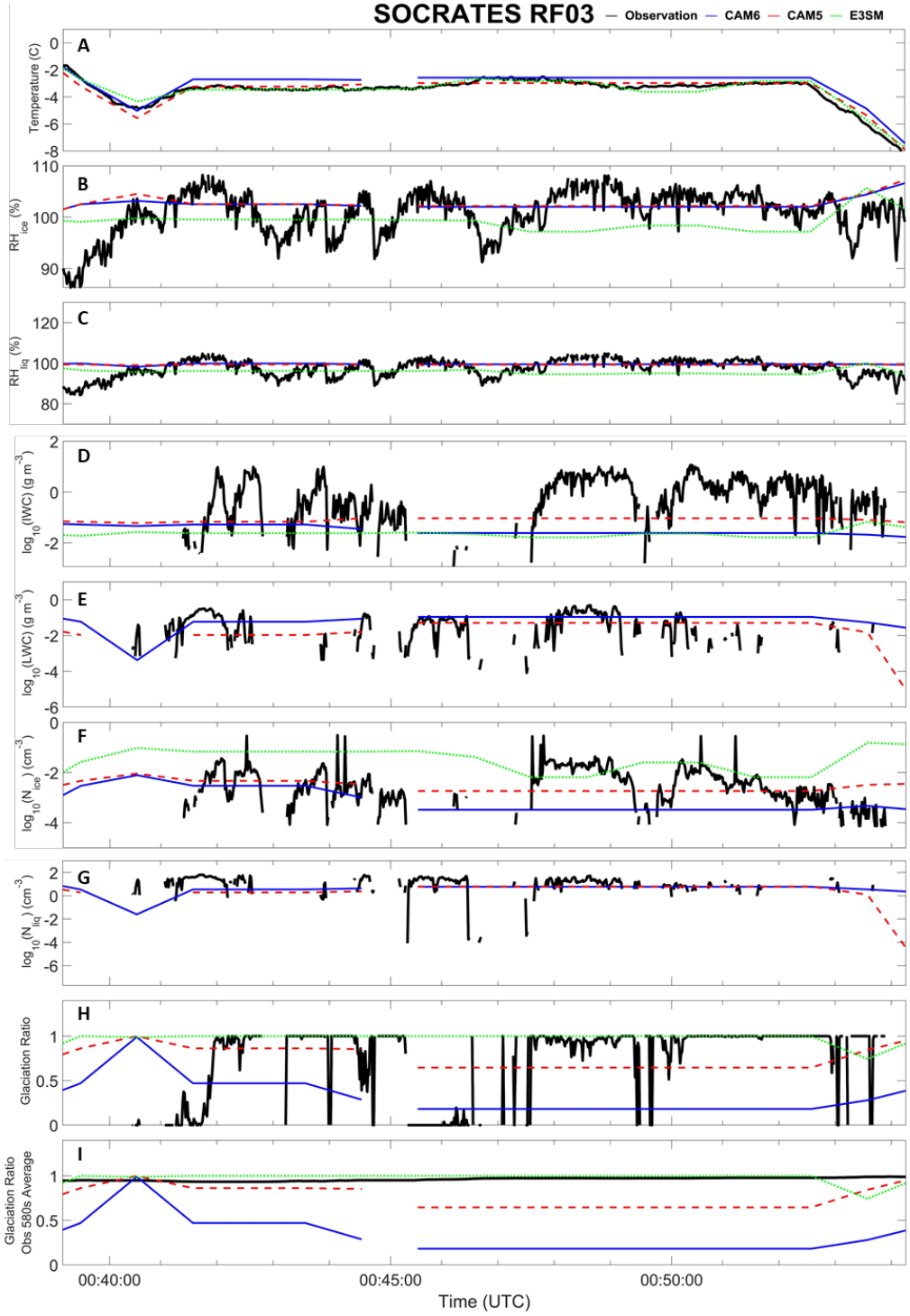

Figure 7. Similar to Figure 3 but for RF03.

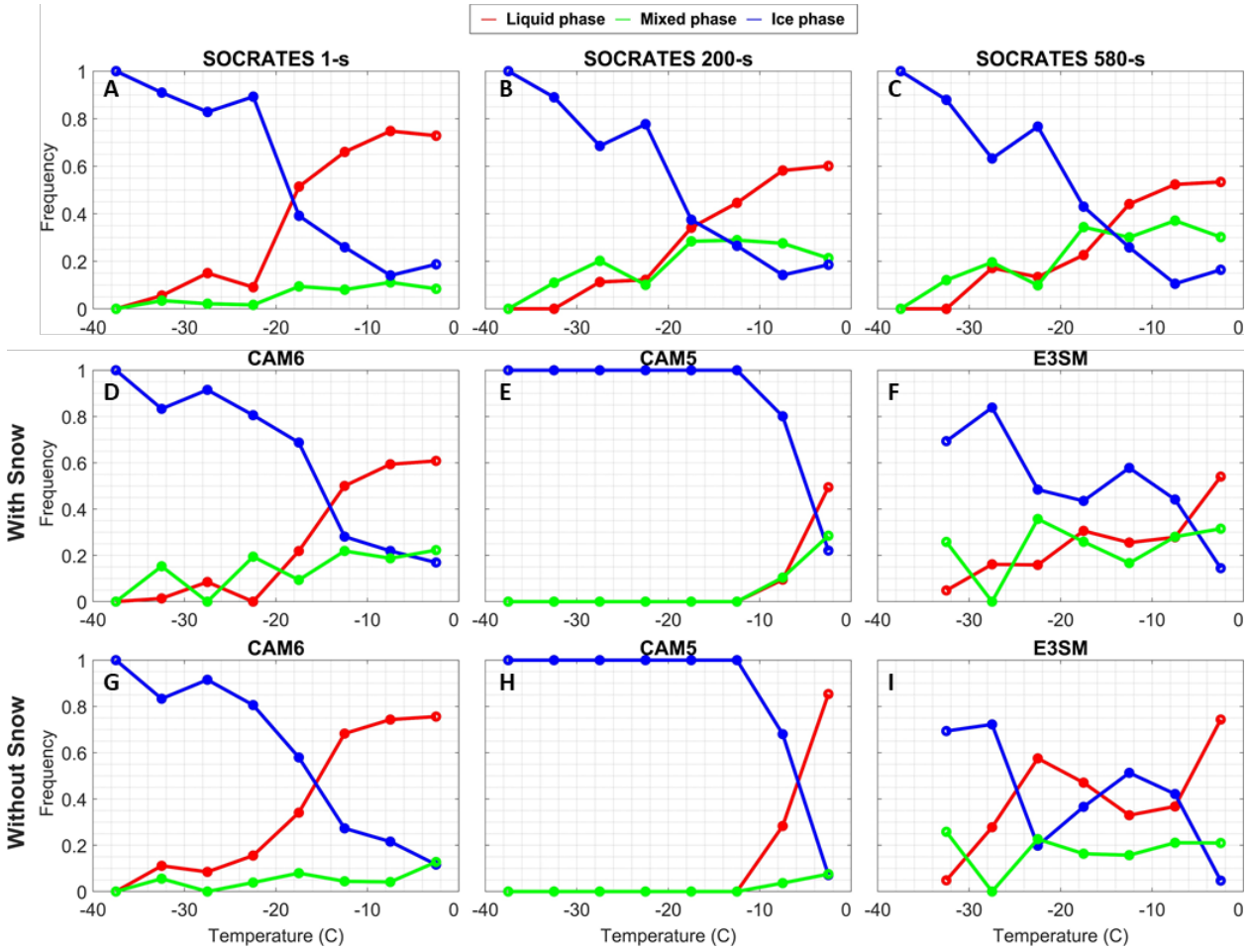

Figure 8. Cloud phase occurrence frequencies for (a) 1-Hz SOCRATES observations, (b) 200-s averaged observations, and (c) 580-s averaged observations with temperature ranged from -40°C to 0°C, binned by 5°C. Cloud phase occurrence frequencies for CAM6, CAM5, and E3SM are shown for two types of simulated IWC: (d – f) including snow and (g – i) excluding snow. Liquid, mixed, and ice phase are denoted by red, green, and blue colors, respectively.

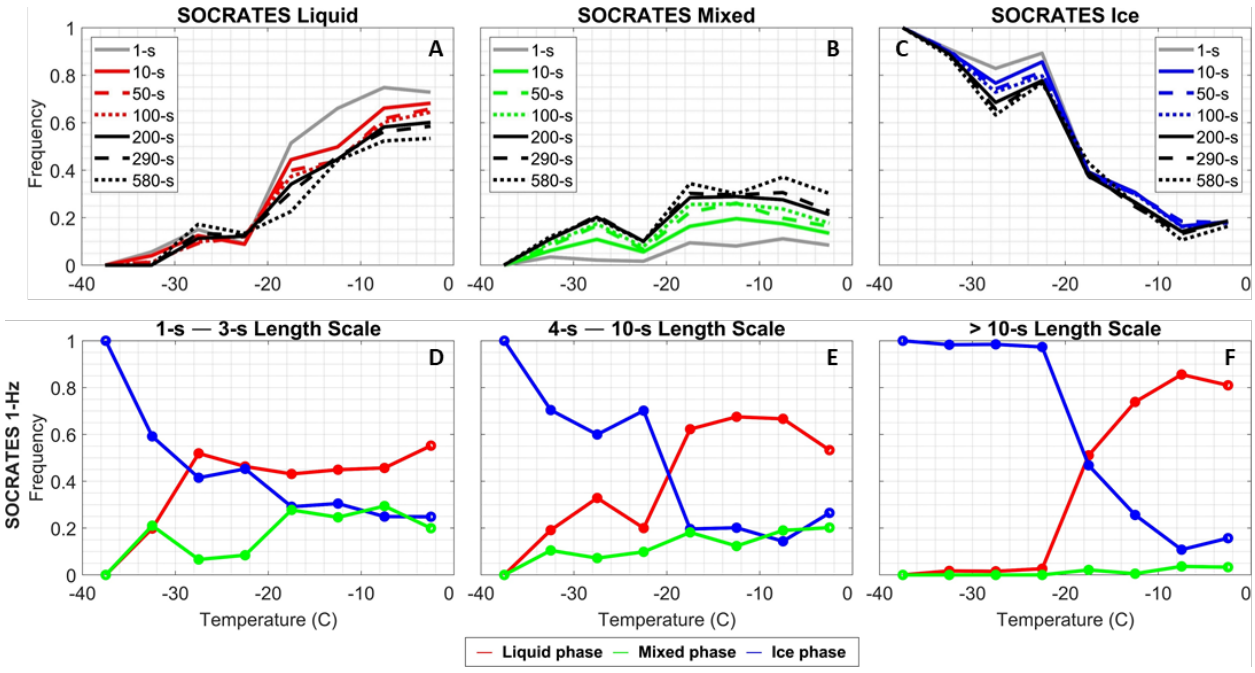

Figure 9. Cloud phase occurrence frequencies for (a) liquid phase, (b) mixed phase, and (c) ice phase are shown for 1-s, 10-s, 50-s, 100-s, 200-s, 290-s, and 580-s averaged observations. (d – f) Occurrence frequency of various length scales of cloud phase, calculated based on 1-Hz observations, including (d) 1-s – 3-s length scale, (e) 4-s – 10-s length scale, and (f) more than 10-s length scale.

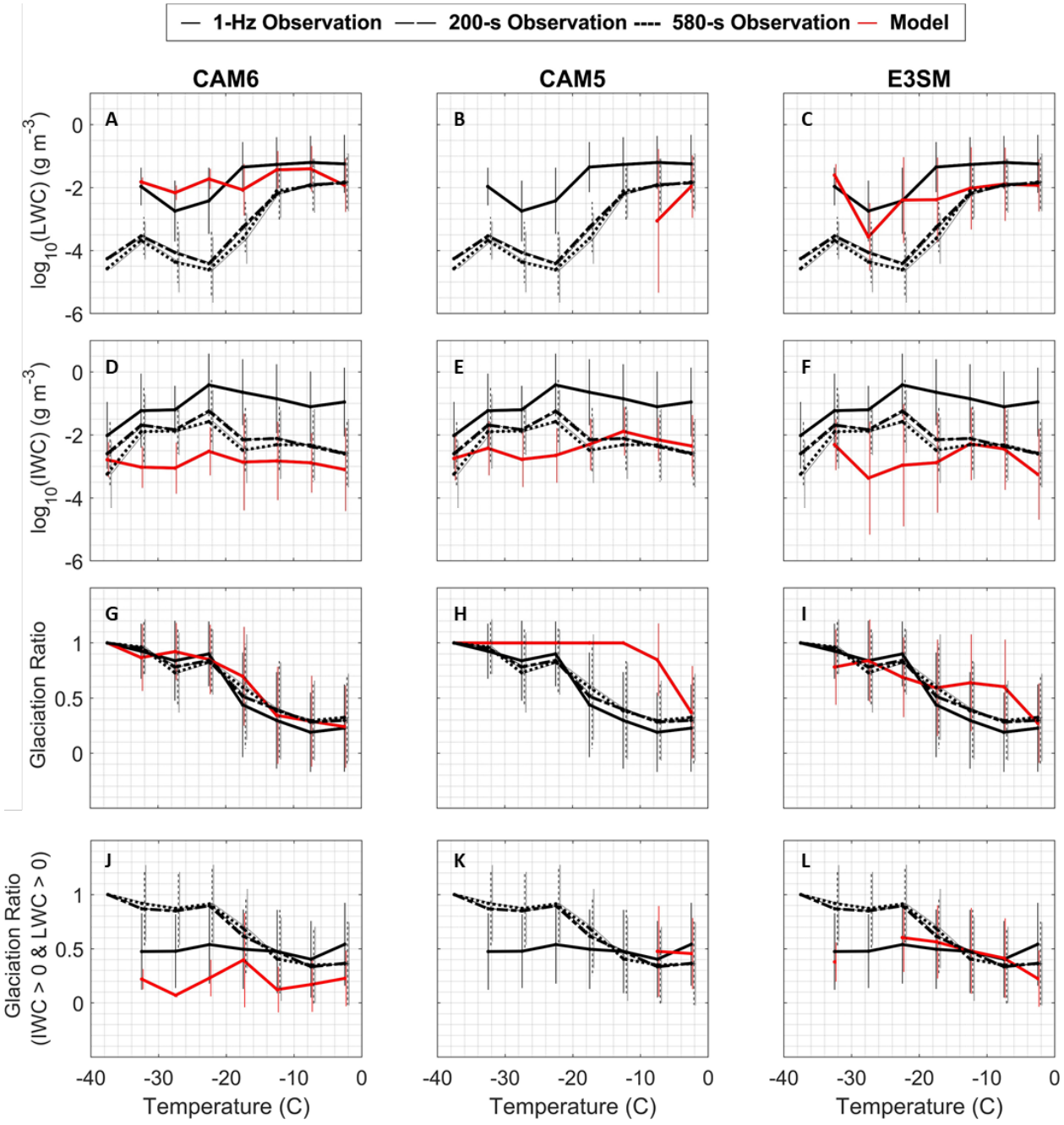

824

825 Figure 10. Averages and standard deviations of (a – c) log-scale LWC, (d – f) log-scale IWC, (g –
826 i) glaciation ratio (i.e., IWC/CWC), and (j – l) glaciation ratio only when ice particles and
827 supercooled liquid water coexist (i.e., IWC/CWC only when both IWC > 0 and LWC > 0). 1-Hz
828 observations (solid black), 200-s observations (dashed black), 580-s observations (dotted black),
829 and model simulations (red) are binned at 5°C interval from -40°C to 0°C.

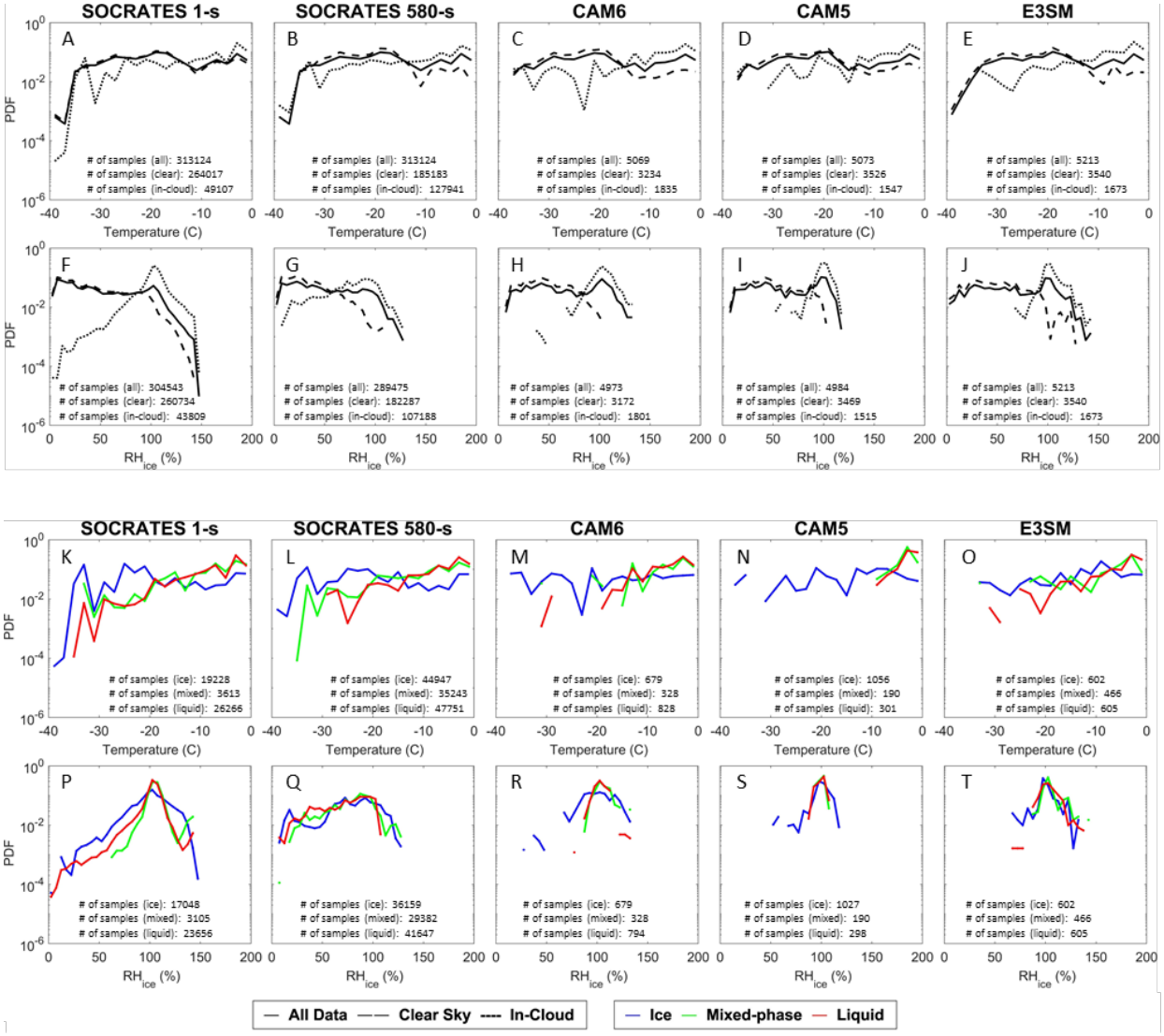

Figure 11. PDFs of (a – e) temperature and (f – j) RH_{ice} for all data (solid black line), clear-sky (dashed black), and in-cloud (dotted black) conditions. PDFs of (k – o) temperature and (p – t) RH_{ice} separated into three cloud phases, i.e., ice (blue), mixed (green), and liquid (red) phase. Each PDF is calculated by the number of a certain condition in a bin divided by the total number of samples of that condition of all bins.

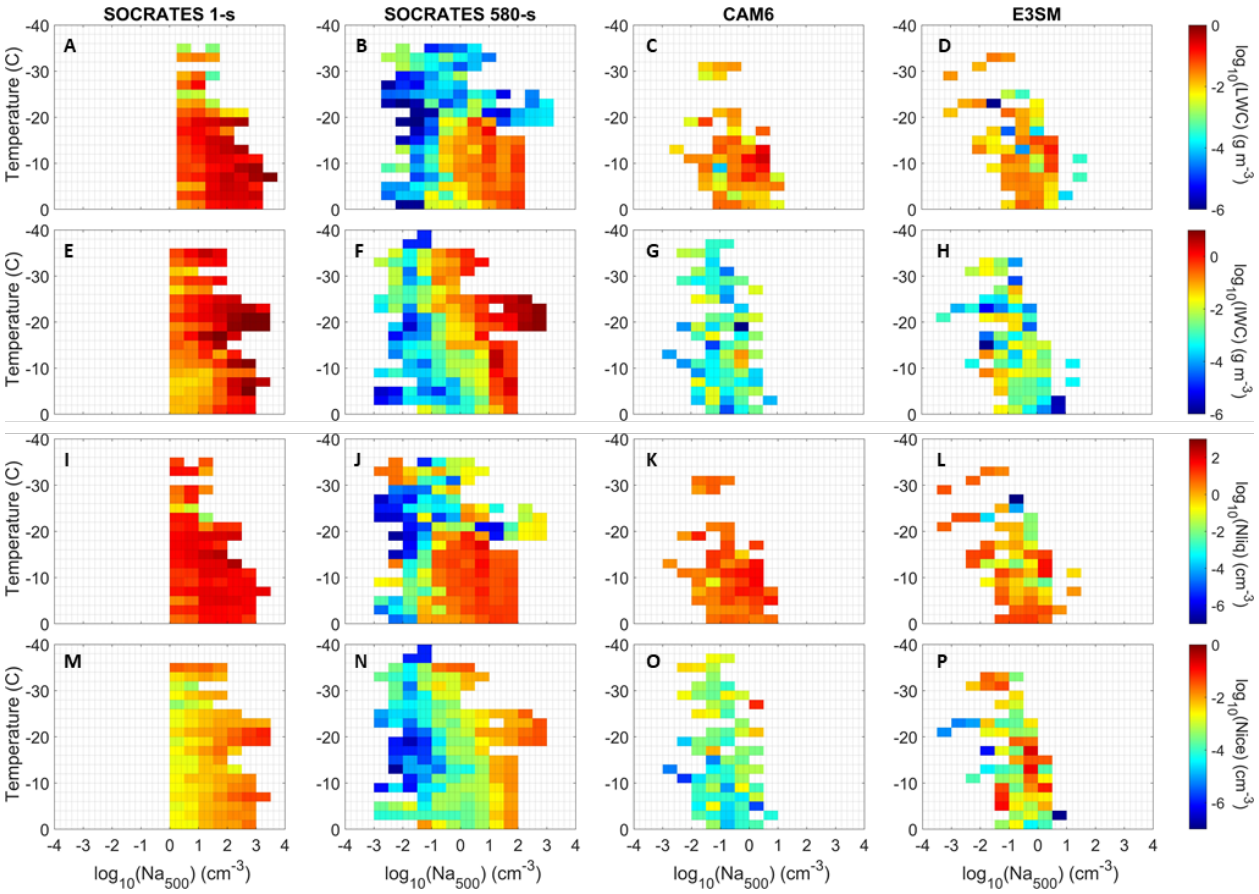

Figure 12. Cloud microphysical properties with respect to logarithmic scale Na_{500} for 1-s observations, 580-s averaged observations, CAM6, and E3SM at various temperatures. Bin colors denote the average of (a – d) $\log_{10}(LWC)$, (e – h) $\log_{10}(IWC)$, (i – l) $\log_{10}(N_{liq})$, and (m – p) $\log_{10}(N_{ice})$.

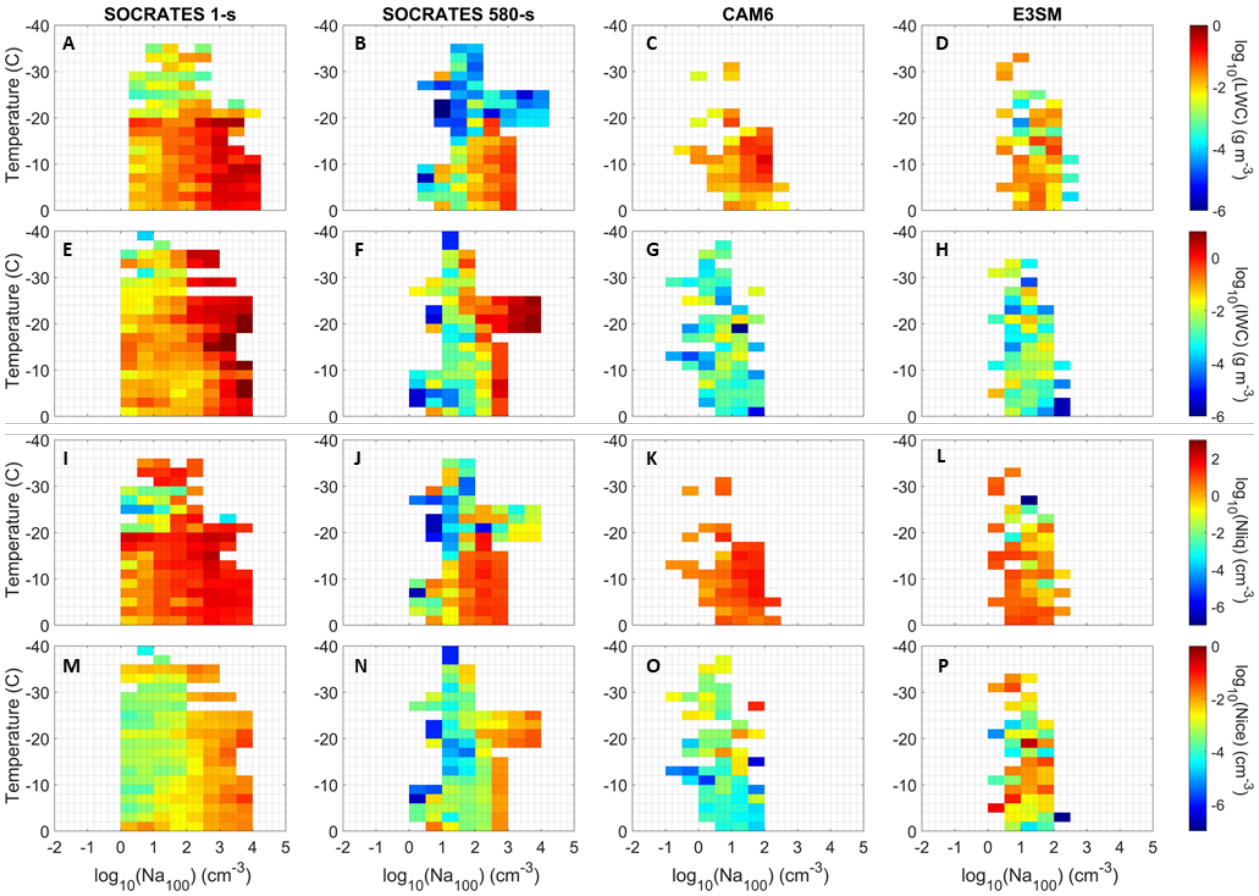

841

842 Figure 13. Similar to Figure 12 but for the relationship with $\log_{10}(Na_{100})$.

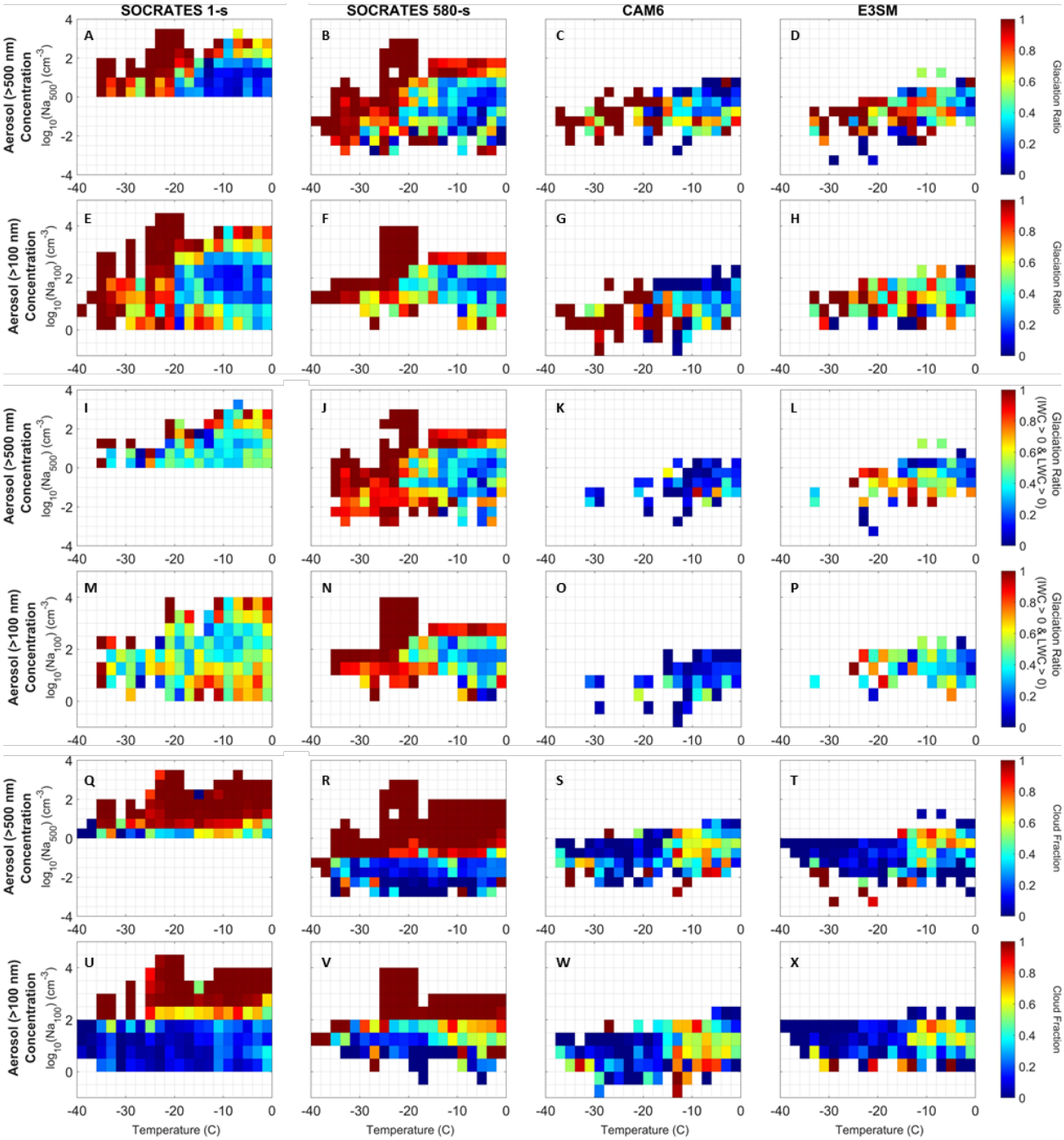

Figure 14. Relationships of (a – h) glaciation ratio of all clouds, (i – p) glaciation ratio only when ice particles and supercooled liquid water coexist, and (q – x) cloud fraction with respect to (row 1, 3, 5) $\log_{10}(Na_{500})$ and (row 2, 4, 6) $\log_{10}(Na_{100})$ at various temperatures. Columns 1 to 4 represent 1-s observations, 580-s observations, CAM6 and E3SM, respectively.